Multiscale Air Quality Simulation Platform (MAQSIP): Initial applications and performance for tropospheric ozone and particulate matter

Rohit Mathur,[1,2,3] Uma Shankar,[1] Adel F. Hanna,[1] M. Talat Odman,[4] John N. McHenry,[5] Carlie J. Coats Jr.,[5] Kiran Alapaty,[1] Aijun Xiu,[1] Saravanan Arunachalam,[1] Donald T. Olerud Jr.,[5] Daewon W. Byun,[6,7] Kenneth L. Schere,[6,3] Francis S. Binkowski,[1] Jason K. S. Ching,[6,3] Robin L. Dennis,[6,3] Thomas E. Pierce,[6,3] Jonathan E. Pleim,[6,3] Shawn J. Roselle,[6,3] and Jeffrey O. Young[6,3]

Received 16 April 2004; revised 9 February 2005; accepted 11 April 2005; published 15 July 2005.

[1] The performance of the Multiscale Air Quality Simulation Platform (MAQSIP) in simulating the regional distributions of tropospheric ozone and particulate matter (PM) is evaluated through comparisons of model results from three-dimensional simulations against available surface and aircraft measurements. These applications indicate that the model captures the dynamic range of observations and the spatial trends represented in measurements. Some discrepancies also exist, however, and they are discussed in the context of model formulation, input data specification and assumptions, and variability and bias in measurements. The daily normalized bias (within ±20%) and normalized gross errors (<25%) for predicted surface level O_3 over an entire summer season are within the suggested performance criteria for management evaluation studies and are comparable to, if not smaller than, those reported previously for other regional O_3 models. Comparisons of modeled PM composition with speciated fine particle concentration measurements show that the model is able to capture the spatial variability in fine PM mass as well as in the inorganic component fractions. Both measurements and model results show that in the summertime in the eastern U.S., SO_4^{2-} is a relatively large component of fine PM mass; in contrast, NO_3^- is a significant fraction in the western U.S. in the wintertime case studied. The ability of the model to simulate the observed visibility indices (extinction coefficient and deciview) are evaluated through comparisons of model estimates using both a detailed Mie theory-based calculation (based on predicted aerosol size and number distributions) and an empirical mass reconstruction algorithm. Both modeled and observed data show that among the various aerosol components, in the eastern U.S. SO_4^{2-} contributes the largest fraction to the aerosol extinction (35–85%), while organic mass contributes up to 20–25%. In contrast, in the western U.S., SO_4^{2-} and NO_3^- have comparable contributions (20–50%) to the observed aerosol extinction. Comparisons with limited observational aircraft data, however, show moderate to poor correlation with measurements in the free troposphere. While these discrepancies can be attributed in part to model initialization and lateral boundary conditions specification, there is a need for further evaluation of the representation of boundary layer-free troposphere exchange mechanisms as well as the chemical mechanisms currently used in the model for representing chemistry in the free troposphere.

Citation: Mathur, R., et al. (2005), Multiscale Air Quality Simulation Platform (MAQSIP): Initial applications and performance for tropospheric ozone and particulate matter, *J. Geophys. Res.*, *110*, D13308, doi:10.1029/2004JD004918.

[1]Carolina Environmental Program, University of North Carolina at Chapel Hill, Chapel Hill, North Carolina, USA.

[2]Now at Atmospheric Sciences Modeling Division, Air Resources Laboratory, National Oceanic and Atmospheric Administration, Research Triangle Park, North Carolina, USA.

[3]On assignment to National Exposure Research Laboratory, U.S. Environmental Protection Agency, Research Triangle Park, North Carolina, USA.

[4]Georgia Institute of Technology, Atlanta, Georgia, USA.

[5]Baron Advanced Meteorological Systems, Raleigh, North Carolina, USA.

[6]Atmospheric Sciences Modeling Division, Air Resources Laboratory, National Oceanic and Atmospheric Administration, Research Triangle Park, North Carolina, USA.

[7]Now at University of Houston, Houston, Texas, USA.

0148-0227/05/2004JD004918$09.00

1. Introduction

[2] Over the past 2 decades, several urban-to-regional-scale atmospheric chemistry-transport models (CTMs) have been developed to study distributions of atmospheric pollutants and relate source emissions to receptor air quality [e.g., *McRae et al.*, 1982; *Lamb*, 1983; *Chang et al.*, 1987; *Venkatram et al.*, 1988; *Morris and Myers*, 1990; *Carmichael et al.*, 1991; *McKeen et al.*, 1991; *Yamartino et al.*, 1992; *Lu et al.*, 1997]. Detailed comparisons of the features of these models can be found in the reviews by *Seigneur and Saxena* [1990], *Peters et al.* [1995], and *Russell and Dennis* [2000]. In many cases the models, along with associated processing systems, were developed to address specific air pollution problems and, in general, represented the state of the science at their inception. Further advances in each of the models have occurred over the years, but a limiting factor in their evolution has been the individual software architecture coupled to the availability of computational resources. Consequently, the design of these models has been based on getting the most practical process representation given the computational restrictions. However, in recent years substantial strides have been made in computational technology that can now facilitate the inclusion of more detailed process representations, advanced parameterizations, and more accurate numerical methods in the models.

[3] In this paper we summarize results from several initial applications of the Multiscale Air Quality Simulation Platform (MAQSIP), a comprehensive Eulerian grid-based model for the transport, chemical transformation, and deposition removal of gas- and particulate-phase atmospheric trace constituents. The model has evolved from the conceptual requirements outlined in the work of *Coats et al.* [1993] and *Dennis et al.* [1996] and was, at its inception, a prototype for U.S. EPA's evolving Models-3 Community Multiscale Air Quality (CMAQ) model [*Byun and Ching*, 1999]. The model has been designed to study current scientific issues related to ozone, airborne acids, and particulate matter (PM) at scales ranging from urban to intercontinental, in a flexible and modular framework that permits detailed comparison of the adequacy of alternative process algorithms, and to evaluate scientific understanding of new process formulations. This paper presents tests of model performance for tropospheric ozone (O_3) and related photochemical species, particulate matter, and visibility estimates that compare model simulations with measurements from a variety of surface- and aircraft-based platforms available for the individual simulation periods. The following section presents a summary of the various physical and chemical processes and their numerical representations in these applications.

2. Model Description

[4] MAQSIP solves the basic mass conservation equation for trace gases and the moment dynamic equations (MDEs) for two or three moments (number and volume, or number, surface area, and volume) for various "modes" (subpopulations) of the particulate size distribution in three dimensions as given in equations (1a) and (1b). The governing species continuity equation (flux-form) in generalized coordinates can be expressed [*Srivastava et al.*, 1994] as

$$\frac{\partial}{\partial t}\left(\sqrt{\gamma}\,\overline{c_i}\right)+\frac{\partial}{\partial x^j}\left(\sqrt{\gamma}\,\overline{c_i}\,\overline{v^j}\right)+\frac{\partial}{\partial x^j}\left(\sqrt{\gamma}\,\overline{c_i'}\,\overline{v^{j'}}\right) = \sqrt{\gamma}R_i+\sqrt{\gamma}S_i,(j=1,2,3), \tag{1a}$$

where γ is the determinant of the metric tensor; c_i is the concentration (mass/volume) of pollutant i; x^j is the jth coordinate; v^j is the contravariant velocity (i.e., the component of the velocity vector in the x^j direction); R_i is the chemical formation or loss rate of pollutant i; S_i is the source/sink term for pollutant i; the overline denotes the mean; and the prime symbol denotes fluctuation about the mean. The determinant of the metric tensor encapsulates the coordinate transformations between the physical and computational space. This formulation allows MAQSIP to accommodate the commonly used horizontal map projections (i.e., Lambert conformal, polar stereographic, and Mercator) as well as various vertical coordinates. In applications over the United States presented here, the model uses the Lambert conformal mapping, and a non-hydrostatic sigma-P coordinate system.

[5] The MAQSIP MDE for M_{ki}, the kth moment of the ith mode of the particulate size distribution, is expressed similar to equation (1a) [*Binkowski and Shankar*, 1995] as

$$\frac{\partial}{\partial t}\left(\sqrt{\gamma}\,\overline{M}_{ki}\right)+\frac{\partial}{\partial x^j}\left(\sqrt{\gamma}\,\overline{M}_{ki}\,\overline{v^j}\right)+\frac{\partial}{\partial x^j}\left(\sqrt{\gamma}\overline{M_{ki}'}\,\overline{v^{j'}}\right) = \sqrt{\gamma}\left(S_{ki}+G_{ki}+C_{kii}+C_{kij}+E_{ki}\right), \tag{1b}$$

where S_{ki} is the rate of change for the kth moment of the ith mode due to cloud processes, G_{ki} is the condensational growth rate for the kth moment of the ith mode, C_{kii} is the unimodal coagulation rate for the kth moment of the ith mode, C_{kij} is the bimodal coagulation rate for the kth moment between modes i and j, and E_{ki} is the emission rate for the kth moment of the ith mode, computed from the emission rates of the fine- and coarse-mode species. The model configuration used in this work assumes a fixed geometric standard deviation of the size distribution in each of three modes and predicts its zeroeth moment (equivalent to number concentration) and third moment (proportional to volume). Modes are distinct populations of aerosols; these applications use a total of three modes to represent the aerosol size distribution. These comprise the fine aerosol modes, formed mainly by secondary chemical processes, spanning the Aitken and accumulation mode size ranges (typically $0.001-1$ μm in median diameter), and the coarse aerosol mode, formed mainly by mechanical processes (and typically $1-10$ μm in median diameter). Section 2.5 contains details of the governing processes in the right-hand side of equation (1b).

[6] Key input variables to MAQSIP are a comprehensive set of emissions and meteorological variables. The modular design of MAQSIP permits a number of choices in the algorithm used for each modeled process. Several of these have been evaluated in detail during the course of the model development; their descriptions and results of the evaluations can be found in the online technical

note available at http://cf.unc.edu/cep/empd/pub_files/maqsiptechnote.pdf, and in references therein. In the following we summarize the salient features of the algorithms used in the applications presented in this work.

2.1. Transport Processes

2.1.1. Advective Transport

[7] The model solves the three-dimensional (3-D) advection equation by using time-splitting [*Yanenko*, 1971] to separate it into locally one-dimensional equations. Alternating the sequence of operations helps reduce time-splitting errors to yield a quasi-second-order accurate solution [*Byun et al.*, 1999]. The applications in this paper have used a positive-definite and monotonic advection scheme by Bott [*Bott*, 1989a, 1989b] due to its relatively high accuracy in conserving mass, minimal numerical diffusion and phase errors, and modest computational costs. In addition, to ensure mass-consistent coupling to the 3-D wind fields input to the model, MAQSIP uses an adjustment of the vertical wind component wherein the vertical velocities are rediagnosed using an inverse donor cell scheme following *Odman and Russell* [2000].

2.1.2. Turbulent Mixing

[8] MAQSIP treats the processes of both horizontal and vertical diffusion. Four boundary layer schemes are currently available for representing the subgrid-scale vertical turbulent mixing of trace species in MAQSIP; two are based on the concepts of eddy diffusivity, and two are based on mixing rates/potentials [*Alapaty and Mathur*, 1998]. The applications presented here used the eddy-diffusivity scheme described in *Chang et al.* [1987], a first-order local-closure scheme, wherein the coefficient of eddy diffusivity is estimated using nonlocal parameters (i.e., noncontiguous in space, such as planetary boundary layer [PBL] height), while the vertical diffusion/mixing is performed locally, between two adjacent vertical layers. For the free troposphere, turbulent mixing is parameterized using the formulation suggested by *Blackadar* [1976].

[9] Horizontal mixing resulting from turbulent fluctuations in the horizontal wind field is parameterized in MAQSIP based upon the eddy diffusivity equation formulated by *McRae et al.* [1982], which can be simplified to yield the horizontal contravariant diffusivities as a function of the horizontal eddy diffusivity, K_h. Specification of K_h must take into account the implicit numerical diffusion in advection [*Yamartino et al.*, 1992; *Odman et al.*, 1997], which in turn is related to the grid size, wind speed, and concentration gradients. *Odman et al.* [1997] provide a quantitative analysis of numerical diffusion for selected advection schemes, along with a guidance for specifying K_h. Given the uncertainties associated with scale dependency of horizontal diffusion, our applications use a spatially uniform K_h, whose magnitude depends on the grid resolution.

2.2. Gas-Phase Chemistry

[10] Two chemical mechanisms, the Regional Acid Deposition Model (RADM) Version 2 (RADM2) [*Stockwell et al.*, 1990] and an updated version of the Carbon Bond Mechanism-IV (CBM-IV) [*Gery et al.*, 1989], are available to represent the tropospheric gas-phase chemical transformations in MAQSIP. The ozone simulations presented here used a version of the CBM-IV mechanism, which includes updates consistent with current consensus kinetics knowledge. These include updated kinetic data for the CO + OH reaction [*DeMore et al.*, 1994] and for PAN chemistry [*Chang et al.*, 1996], an updated condensed isoprene chemical mechanism based on *Carter* [1996], and modifications to the chemical pathways of universal peroxy radical operators (XO2 and XO2N) used in the CBM-IV mechanism. The additional XO2 + HO_2 reaction proposed by *Dodge* [1989] is included to improve the H_2O_2 yields in this mechanism. Also, three additional XO2N reactions (XO2N + HO_2, XO2N + XO2, and XO2N + XO2N) are considered. Studies with these modifications indicate that these terminal reactions can significantly affect simulated regional NO_x and O_3 concentrations [*Kasibhatla et al.*, 1997]. The RADM2 mechanism has also been extended for PM simulations to include oxidation pathways for formation of secondary organic aerosol (SOA) from anthropogenic volatile organic compound (VOC) precursors (higher alkanes, internal alkenes, and aromatics [cresols, xylene, and toluene], and biogenic precursors [monoterpenes] whose oxidation by OH, O_3, and NO_3 mimics that of olefins). The separation of the biogenic and anthropogenic components of olefins allows better representation in the seasonal variability of monoterpene emissions, estimated from BEIS3, U.S. EPA's state-of-the-science Biogenic Emissions Inventory System Version 3 [*Vukovich and Pierce*, 2002]. The numerical integration of the ordinary differential equations representing the gas-phase kinetics is performed using a modified version of the quasi-steady state approximation (MQSSA) scheme as described by *Mathur et al.* [1998] that can be used with any chemical mechanism. The chemistry integration time steps are determined internally based on local stiffness of the chemical system, such that the chemistry is integrated for the duration of the model time step in the time-splitting mode. Additional details on the performance and accuracy of the scheme are described by *Mathur et al.* [1998].

2.3. Photolysis Rates

[11] The calculation of photolysis rates in clear air and in clouds requires the specification of wavelength bands, extraterrestrial irradiance, surface albedo, ozone profiles, aerosol profiles, cloud distributions, and absorption cross section and quantum yield data. The absorption cross section and quantum yield data are derived from experiments and are well documented and updated periodically [e.g., *DeMore et al.*, 1994]. MAQSIP uses photolysis rates from a lookup table following *Chang et al.* [1987]. It is constructed from the delta-Eddington radiative transfer model [*Madronich*, 1987] and consists of photolysis rates at specific altitudes, latitudes, and hour angles. The model linearly interpolates these values in space and time to calculate the clear-sky photolysis rates in each grid cell. Cloud fraction, cloud altitude and thickness, and cloud optical depth derived from the model's cloud scheme, described in the next section, are used to calculate attenuation due to clouds.

2.4. Cloud Processes

[12] The cloud process equation in MAQSIP represents the rate of change of the species concentration due to the presence of clouds in a given grid column as a sum of the

rates of change due to subgrid-scale vertical turbulent mass flux divergence generated by deep convection and shallow convection, the aqueous-chemical formation/loss due to kinetic production/destruction of dissolved species, and loss due to precipitation removal. The formulation represents the superposition of effects of clouds of different morphologies that may occur within a grid column and depends on the horizontal resolution of the simulation. Three spatial resolution ranges are covered in the model's cloud process parameterizations; regional scale, mesoscale, and urban scale.

[13] For regional-scale applications (typically $\geq$60 km), MAQSIP uses the RADM Version 2.61 cloud scheme [*Chang et al.*, 1990; *Dennis et al.*, 1993; *McHenry and Dennis*, 1994], and includes treatment of precipitating and nonprecipitating (pure fair weather, or coexisting with precipitating) clouds; these latter cloud types are important for representing sulfate production, as they provide no wet removal mechanism and very efficient SO_2 oxidation pathways relative to clear air. For the deep convective (precipitating) clouds, the RADM analytical package is used, while for the latter the mixing mechanism described by *Dennis et al.* [1993] is used. Aqueous chemistry, followed by wet deposition, is calculated as in the work of *Chang et al.* [1990] and *Walcek and Taylor* [1986] if the vertically averaged cloud liquid water content (LWC) exceeds 0.01 gm^{-3}, otherwise reactivity is ignored. This typically occurs when cloud temperatures are below freezing. In that case wet removal is modeled as an exponential following *Giorgi and Chameides* [1985]. This scheme is used in the PM model applications because currently this is the only convective scheme available in MAQSP that is linked to the RADM aqueous chemical species.

[14] For mesoscale applications (typically between 12 and 60 km), MAQSIP uses a version of the Kain-Fritsch scheme [*Kain and Fritsch*, 1990, 1993] for deep convection. This scheme in MAQSIP can mimic the cloud triggering data, time of onset, and cloud duration using saved data from the driving meteorological model. The convective mass flux is used to estimate fractional coverage following *Xu and Krueger* [1991], and the vertical extent and cloud liquid water. These are then used to calculate the cloud optical depth, which is used for estimating the attenuation of photolysis rates due to clouds. The aqueous chemical mechanism treats dissolution and dissociation of gases similar to *Walcek and Taylor* [1986], and employs a simplified chemistry including N_2O_5 hydrolysis that is appropriate for simulating tropospheric ozone and wet removal of dissolved pollutants. This scheme is used in the 36-km and 12-km ozone simulations presented subsequently.

[15] All model applications also use a resolvable-scale cloud scheme wherein the cloud is resolved by the driving meteorological model. This can occur at any grid resolution, and for such clouds, no additional cloud dynamics are considered, since any convection and mixing would have been represented in the wind fields. MAQSIP assumes the presence of resolved-scale cloud when condensed water exceeds 0.05 g kg^{-1} in a given model grid cell, which represents about one-tenth that needed for autoconversion to precipitation. Aqueous chemistry is carried out for all condensate concentrations exceeding this value in a given model grid cell, and wet removal is computed when precipitation falls. At urban scales, i.e., grid resolutions typically finer than 4 km, no other convective parameterizations are invoked. The cloud optical depth is calculated using the approach described by *Hansen et al.* [1983]. The clear-sky photolysis values are then modified according to *Chang et al.* [1987]. To treat the presence of multiple cloud types within a grid column, an alternative scheme to compute an average attenuation factor weighted by the cloud fraction for each cloud type in the grid column is also available [*Shankar et al.*, 1999].

[16] For PM applications, MAQSIP's cloud model also includes in-cloud scavenging of the aerosols, their dissolution in cloud droplets, the increase of aerosol mass due to sulfate production, and their wet deposition [*Binkowski and Shankar*, 1994; *Shankar and Binkowski*, 1994]. The rate of change of aerosol moments is derived in terms of the in-cloud scavenging rate due to Brownian coagulation of interstitial particles with cloud droplets, the wet removal rate, and the production rate of SO_4^{2-} mass as an extension of the two-step process of *Slinn* [1974] and *Chaumerliac* [1984].

2.5. Particulate Processes

2.5.1. Size Distribution Representation

[17] MAQSIP models the size distributions of particulate species using the modal approach described by *Binkowski and Shankar* [1995], wherein the aerosol populations representing two fine modes (Aitken, accumulation) and a coarse mode are mathematically modeled as a superposition of three lognormal functions that evolve in size space with time. These applications use fixed geometric standard deviations that have been set to 1.7, 2.0, and 2.2, respectively, in each mode. The geometric mean diameter of each mode is diagnosed from the predicted moments at each model time step for size-dependent calculations, e.g., coagulation rates, deposition velocities, and visibility metrics. Species treated in the applications shown here are NH_4^+, primary and secondary SO_4^{2-} and NO_3^-, primary and secondary organic carbon (OC) primary elemental carbon (EC), and fugitive dust; all are distributed in the fine and coarse modes, with the exception of secondary OC, and the inorganic species, which are treated only in the fine modes. The coarse mode is assumed not to undergo any chemical processing. Additionally, coagulation is omitted in this mode due to its relatively low number concentrations. Thus the coarse mode in the applications presented here changes only in response to emissions and to wet and dry removal.

2.5.2. Aerosol Dynamics

[18] The moment dynamic equations are solved for the moments of the distribution using size-dependant coagulation and condensation growth rates as described by *Whitby et al.* [1991]. The change in aerosol moments due to the growth of particles by condensation of vapor-phase sulfate and organics, and by the homogeneous nucleation of sulfuric acid and water, is represented as a coupled process, where nucleation occurs only as long as the steady-state sulfate concentration exceeds the critical concentration [*Binkowski and Shankar*, 1995]. Zeroeth- and third-moment production rates due to nucleation are calculated based upon the condensation timescale and the production rate of sulfate vapor from SO_2 oxidation, following the nucleation parameterization scheme of *Harrington and Kreidenweis*

[1998]. This scheme uses the vapor production rate to predict the critical vapor concentration above which nucleation occurs, and independently calculates the nucleation rates for the two moments in the Aitken mode, treated as the repository of new particles. The vapor mass remaining that does not go into new particle formation is condensed onto existing particles; thus, the difference between the vapor production rate and nucleation rate for the third moment is used to compute the growth rates due to sulfate condensation for the third moments of the chemically active aerosol modes, following *Whitby et al.* [1991]. These rates are added to those due to anthropogenic and biogenic SOA production, calculated using yield fractions (i.e., the mass concentration of SOA produced per unit mass concentration of the VOC reacted) given by *Pandis et al.* [1992, 1993], and the concentrations of the precursor organic groups. Primary emission rates for aerosol species such as fine and coarse dust and organic and elemental carbon are converted into emission rates for the aerosol moments using the background values of the size parameters for the accumulation and coarse modes and added to the overall moment rate of change. The constituent aerosol species themselves are updated for emissions in the vertical diffusion algorithm.

[19] The moment dynamic equations are solved using a forward Euler integration scheme described by *Whitby et al.* [1991]. The subsequent diagnosis of the mode mean diameters may show strong overlap between the modes due to the impact of the dynamic processes on particle growth. To preserve the distinctness of two prognostic fine modes, a fraction of the moments of the Aitken mode is transferred to the accumulation mode using the overlap criteria described by *Binkowski* [1999].

2.5.3. Thermodynamics of Inorganic Species

[20] Inorganic aerosol composition in these applications is determined using the Regional Particulate Model Aerosol Reacting System (RPMARES) described by *Binkowski* [1999]. The model treats the bulk equilibrium of the SO_4^{2-}-NO_3^--NH_4^+-H_2O system with the gas phase, assuming the particles to be in the metastable state, i.e., the particles are assumed to never dry out. The particulate-phase species concentrations after equilibrium are partitioned among the Aitken and accumulation modes proportional to the sulfate mass in the modes. The ISORROPIA thermodynamic model has recently been added to the available model options, and found to compare very closely to the performance of RPMARES for the inorganic species [*Shankar and Mathur*, 2001]. In applications with ISORROPIA, the MAQSIP aerosol chemistry has been modified to model the interaction of sea salt species (Na^+, Cl^-) with anthropogenic species in the fine and coarse modes [*Shankar and Mathur*, 2003] (also see http://www.cmascenter.org/2003_workshop/session4/shankar_presentation.ppt).

2.6. Dry Deposition

[21] The species deposition velocity, v_d, is used to estimate the deposition flux to the surface, $F_d = \sqrt{\gamma} v_d c$, where c is the model concentration in the lowest model layer. This flux is treated as a bottom boundary condition in vertical turbulent mixing calculations for both gases and aerosols. The deposition velocity is parameterized in terms of physical, chemical, and vegetative factors, and is estimated following a method analogous to resistance in series [*Wamsley and Wesely*, 1996]. Size-dependent dry deposition velocities for the fine and coarse aerosol moments and constituent species are computed following the surface-layer resistance method described by *Binkowski and Shankar* [1995].

2.7. Visibility Analysis

[22] MAQSIP outputs of PM species concentrations and size distributions permit the analysis of visibility impairment due to PM. The visual range is defined as the farthest distance at which an observer can distinguish between an object and its background. The contrast between an object and its background is reduced by the light extinction due to absorption and scattering by air molecules and PM in the light path, with the aerosol component (β_{sp}) dominating that due to Rayleigh scattering and absorption by atmospheric gases. Assuming a discernible minimum of 2% for contrast, the relationship of d, the visual range, to the light extinction coefficient (β_{ext}) is given by *Koschmieder* [1924] as

$$d = 3.912/\beta_{ext}. \tag{2}$$

However, these quantities do not exhibit a linear profile with respect to perceived visual changes. A somewhat more useful visibility impairment measure is the deciview (d_v) index, which is directly proportional to the logarithm of light extinction [*Pitchford and Malm*, 1994]:

$$d_v = 10 \ln(\beta_{ext}/0.01) = 10 \ln(391.2/d), \tag{3}$$

with $\beta_{ext} = \beta_{sp} + 0.01$, where 0.01 km^{-1} is the standard value for Rayleigh extinction (corresponding to an average visibility of 391.2 km), and β_{sp} is the aerosol extinction in km^{-1}.

[23] In MAQSIP two methods are available for estimating β_{sp} and d_v. The first method is based on a detailed approach that uses particle size distribution parameters predicted at each model grid cell in conjunction with a Mie scattering algorithm [*Wiscombe*, 1980; *Hanna et al.*, 1993] to estimate aerosol optical properties. The algorithm estimates the light extinction efficiency due to aerosols based on the particle effective radius (half the ratio of the third moment to the second moment of diameter) and refractive index; the aerosol refractive index is adjusted according to the aerosol liquid water content using an empirical fit to the data of *Kim and Boatman* [1990]. The extinction coefficient, β_{sp}, is then computed using the aerosol surface area and number concentration.

[24] When particle size distribution information is not available, as is often the case with monitoring data, a second method based on the empirical algorithm of *Sisler and Malm* [2000] can be used. This allows evaluation of modeled visibility against the Interagency Monitoring of Protected Visual Environments (IMPROVE) network [*Malm et al.*, 1994] estimates. In this method, β_{sp} is given by:

$$\begin{aligned}\beta_{sp} = {} & 0.003 f(\mathrm{RH})([\text{sulfate}] + [\text{nitrate}] + [\text{ammonium}]) \\ & + 0.004([\text{organic mass}]) + 0.01([\text{light-absorbing carbon}]) \\ & + 0.001([\text{fine soil}]) + 0.0006([\text{coarse mass}]),\end{aligned} \tag{4}$$

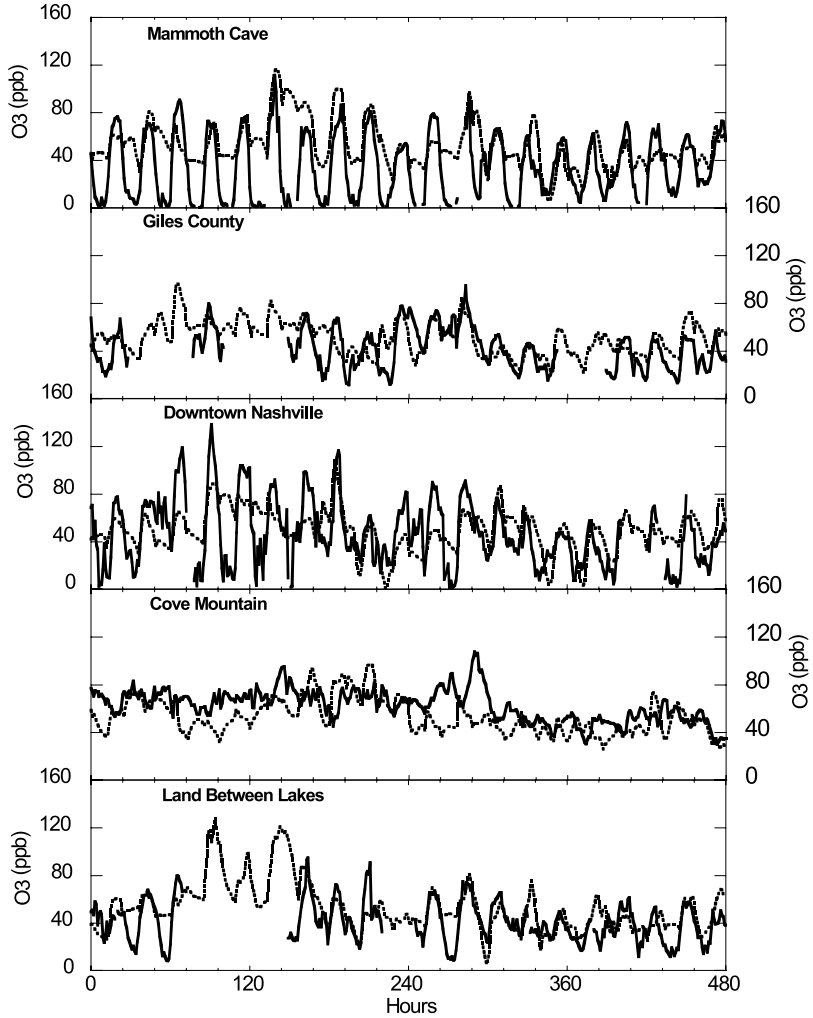

Figure 1. Comparison of hourly variations in surface-level O_3 simulated by the model (dashed) with observations (solid) at selected sites for a 20-day period starting 1200 UTC 7 July 1995.

where mass concentrations of the aerosol constituents are in $\mu g\ m^{-3}$, and f(RH) is a relative-humidity-based correction factor to account for light scattering by the aerosol liquid water, and is based on data presented by *Malm et al.* [1994].

3. Regional Ozone Modeling

[25] While regional-scale atmospheric CTMs have been widely used to study short-term episodes characterized by extreme surface-level O_3 pollution, little effort has been devoted to examining their performance over longer time periods under various dynamical and chemical conditions. The proposed change to the national ambient air quality standard (NAAQS) for O_3 from a maximum 1-hour average concentration to a maximum 8-hour average concentration (http://www.epa.gov/ttn/naaqs/ozone/o3imp8hr) is expected to significantly increase regions of O_3 nonattainment [*Chameides et al.*, 1997] and may require analyses of CTM simulations over longer periods.

[26] In the context of these emerging needs, MAQSIP was used to simulate the distribution of tropospheric O_3, its precursors, and a variety of secondary product species for a full summer season (15 May to 11 September 1995) over the eastern United States (domain comparable to that shown in Figure 7a). The horizontal grid employed a 36-km resolution, and 22 sigma levels were used in the vertical up to 100 mb. Meteorological fields were derived from the Fifth-Generation Penn State/NCAR Mesoscale Model (MM5) [*Grell et al.*, 1994], which was run with four-dimensional data assimilation (FDDA) and reinitialized every five days. The emission inventories of CO, NO_x, and VOCs used in these simulations are described by *Houyoux et al.* [2000].

3.1. Comparison With Surface Measurements

[27] Figure 1 shows comparisons of predicted hourly surface O_3 concentrations against measurements over a 20-day summer period at selected sites from the Southern Oxidants Study [*Meagher et al.*, 1998]. These time series plots allow examination of the model's ability to reproduce the magnitude of diurnal variations in predicted O_3 as well as the timing of the peak O_3, relative to the measurements. It can be seen that while the model captures the daytime peaks at most sites and the variability across the various sites, it overpredicts nighttime O_3. This overprediction can be attributed to a relatively coarse horizontal resolution, a coarse surface-layer vertical resolution (~38 m), and subgrid-scale effects associated

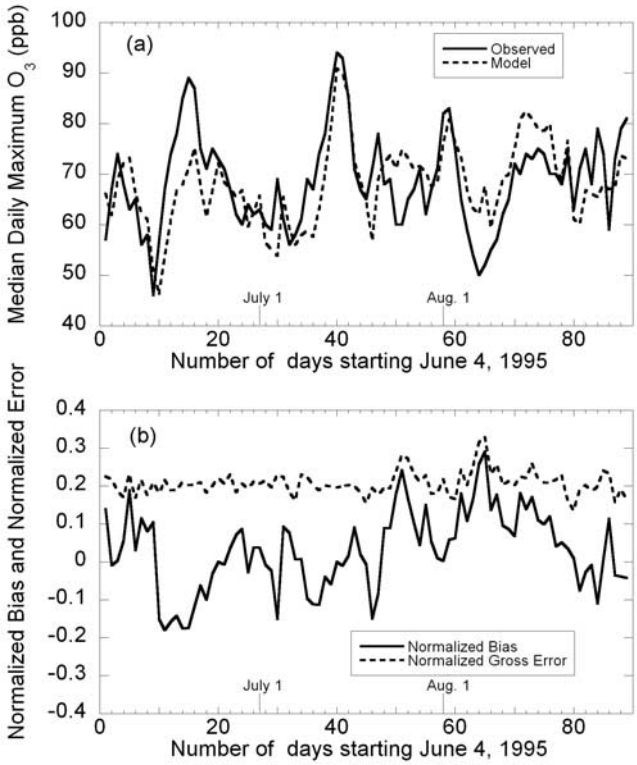

Figure 2. (a) Comparison of variations in modeled and observed domain-median daily maximum O_3. (b) Variations in daily normalized bias and normalized gross error computed using modeled and observed hourly values at 539 AIRS sites in the eastern U.S.

with the representation of O_3 titration by NO_x; the artificial dilution of nighttime surface NO_x emissions over the model grid volume results in underestimation of modeled NO_x concentrations and consequently overprediction in nighttime O_3.

[28] To assess model performance in simulating regional surface O_3 distributions over the eastern United States over the entire summer season, model results were compared with measurements from the Aerometric Information Retrieval System (AIRS) network for a June–August 1995 period; there are 539 AIRS stations within the modeled domain. To illustrate MAQSIP's ability to simulate the interday variability in synoptic surface O_3, Figure 2a presents comparisons of modeled and observed median daily maximum O_3 for the June–August period. The daily maximum O_3 was computed at each of the AIRS sites and the median value across all sites was taken to represent each daily point in Figure 2a; the modeled median value was similarly computed based on daily maximum O_3 at grid cells corresponding to each of the AIRS sites. Comparisons of the daily variations in measured and modeled-domain median maximum O_3 concentrations provide an overall assessment of the model's ability to represent the processes regulating regional O_3 distributions over the 3-month simulation period. As can be seen in Figure 2a, the model replicates the trends in interday O_3 variations. A more quantitative assessment of model performance for surface O_3 is illustrated in Figure 2b, which presents variations in the daily normalized bias (NB) and normalized gross error (NGE), defined as

$$NB = \frac{1}{N}\sum_{i=1}^{N}\frac{(c_i^m - c_i^o)}{c_i^o} \quad (5)$$

$$NGE = \frac{1}{N}\sum_{i=1}^{N}\frac{|c_i^m - c_i^o|}{c_i^o}, \quad (6)$$

where for a given day, N is the number of valid modeled-observed pairs (number of valid stations x number of valid hours in day), and c_i^m and c_i^o are the modeled and observed concentrations, respectively, at station i. In computing the NB and NGE, we used a cutoff value of 40 ppb O_3 for c_i^o, to screen out data pairs with low observed O_3. For most days within the 3-month simulation period (~90%), the bias in predicted surface O_3 is within ±20%, while the normalized gross error is <25%. These daily metrics are within the suggested performance criteria for management evaluation studies [*U.S. Environmental Protection Agency*, 1991] and are comparable to if not smaller than those reported for other regional models by *Russell and Dennis* [2000].

[29] Additional comparisons of MAQSIP-predicted surface O_3 concentrations from these simulations against measurements from the AIRS network have been reported in two recent studies. *Kasibhatla and Chameides* [2000] examined model performance from an episodic perspective by computing modeled-observed correlation coefficients (r) on a day-to-day basis, and also from a seasonal perspective by calculating r on a percentile basis (i.e., at each location a specific percentile of the observed and modeled time series was selected and the r associated with that percentile was computed). Their analyses indicated that although the modeled-observed correlation coefficients computed on a day-to-day basis showed significant variability (0.1–0.8), on a percentile basis the model captured the dynamic range of the observations quite well. The surface O_3 predictions from the seasonal calculations have also been evaluated using spectral decomposition of modeled and observed values into fluctuations on intraday, diurnal, synoptic, and longer-term timescales following the approach of *Rao et al.* [1997]. The correlations between modeled and observed values were found to be low for the intraday component, high for the diurnal component due to the inherent diurnal cycle, and highest for the synoptic and longer-term timescale components [*Hogrefe et al.*, 2001a, 2001b].

3.2. Comparison With Vertical Profile Measurements

[30] To assess the model's representation of the vertical distribution of trace species, model predictions were compared with aircraft measurements. Figure 3 presents modeled and observed vertical profiles for O_3, NO_y, and CO at two locations where aircraft spirals were conducted under the North American Research Strategy for Tropospheric Ozone (NARSTO) program. The aircraft spirals at Poughkeepsie, New York, were conducted in the early morning (0400–0500 EST), while those at Summit, Delaware, were conducted in the afternoon (1400–1500 EST), providing an opportunity to compare and contrast model performance during both daytime and nighttime conditions. While the

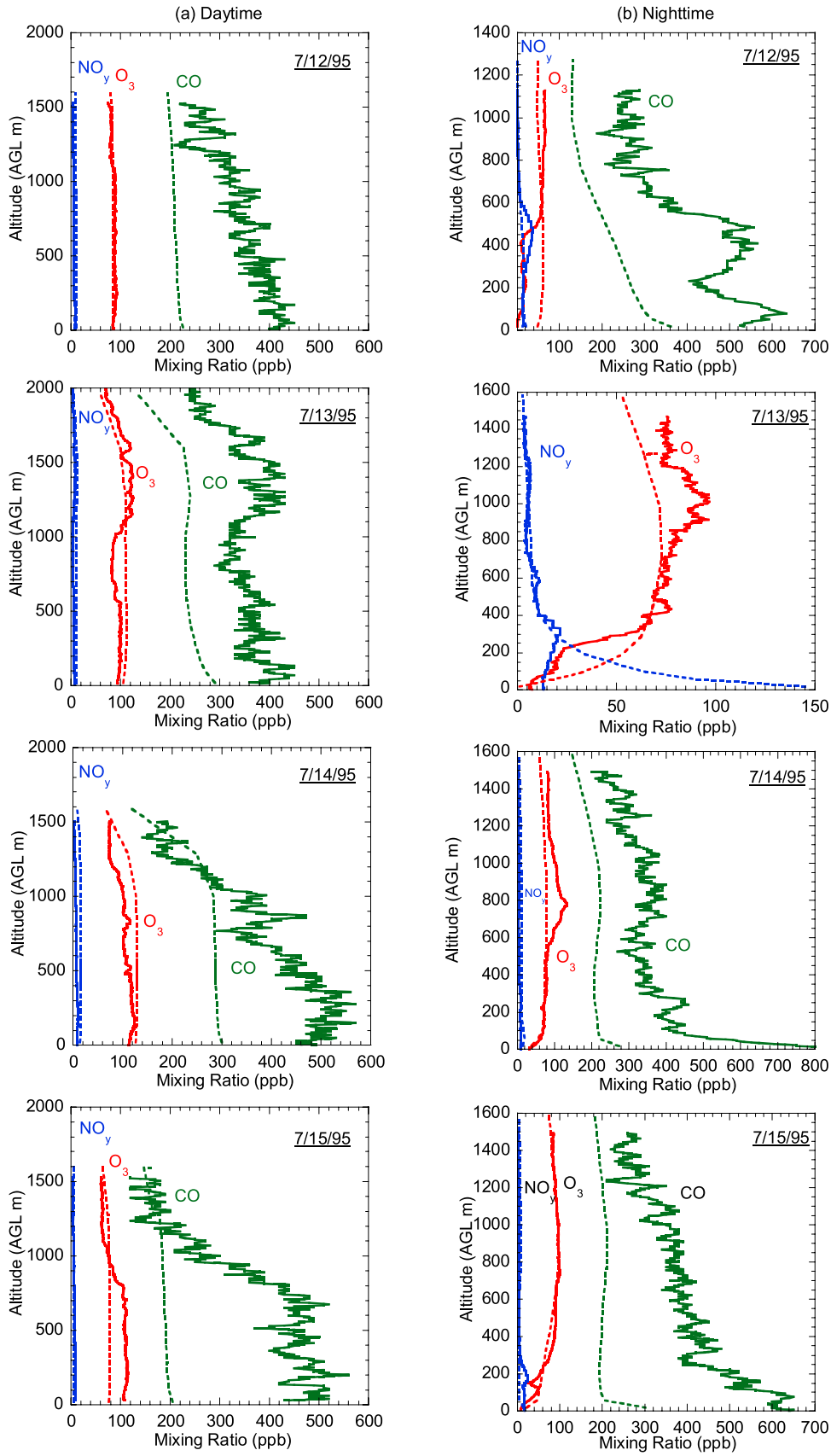

Figure 3. Comparison of modeled (dashed lines) and observed (solid lines) vertical distributions of O_3 (red), CO (green), and NO_y (blue) for different days: (a) daytime profiles at Summit, Delaware; (b) nighttime profiles at Poughkeepsie, New York.

model is able to simulate the general range in individual species concentrations and the qualitative features of the observed vertical profiles (such as well-mixed profiles through the boundary layer during the day and residual layer at night), discrepancies occur between the modeled and observed values on a day-to-day basis. The nights of 12 and 15 July 1995 in particular present stressful tests for the model, as the observations indicate the presence of fresh plumes (high NO_y and low O_3) aloft the nocturnal boundary layer; such features are not likely to be resolved by the dynamics and transport represented on a 36-km grid. Large discrepancies between modeled and observed CO concentrations are also noted at the locations of these aircraft spirals. The high observed CO concentrations between the surface and 2 km altitude probably result from the influence of extensive Canadian wildfires that occurred between June and mid-July 1995, primarily north of 55°N latitude. These emissions, which were outside our model domain, were not considered in these applications, nor were their transport effects reflected in the static lateral boundary conditions used; this could contribute to the noted CO underpredictions. This is further confirmed by recent modeling studies that considered emissions from these wildfires and showed significant improvement in model performance in predicted CO relative to both surface and aloft measurements [cf. *McKeen et al.*, 2002].

3.3. Comparison With Regional Aircraft Measurements

[31] From 21 June through 20 July 1995, measurements of a variety of trace species were made from extensively instrumented aircraft deployed as part of the Middle Tennessee Ozone Study [*Hübler et al.*, 1998]. Measurements onboard the WP-3D aircraft operated by the National Oceanic and Atmospheric Administration (NOAA) cover a broad regional area extending north into Illinois, Indiana, and Ohio, and east into North and South Carolina. These measurements provide an opportunity to evaluate the model's performance both within the daytime boundary layer and above it from a regional perspective and to compare and contrast the simulated and observed chemical composition over regions characterized by different emission source types. Five-minute-averaged data corresponding to the time resolution of the in situ VOC measurements [*Hübler et al.*, 1998] were provided by the NOAA Aeronomy Laboratory. For each flight, model-simulated mixing ratios were extracted by "flying" the aircraft through the 3-D modeling domain for 14 daytime flights; the spatial locations of the aircraft were mapped to the model grid, whereas hourly resolved model outputs were linearly interpolated to correspond to the time at the middle of each 5-min measurement interval.

[32] Correlations between these modeled and observed mixing ratios, which are paired in both space and time, are presented in scatterplots in Figure 4. To differentiate comparisons within the daytime boundary layer (BL) from those in the free troposphere (FT), we segregated the modeled and observed data into two bins using an altitude of 2 km as representative of mean daytime BL height within the study region. This is in general agreement with observations during this period [*McNider et al.*, 1998] as well as the MM5 predictions used here. Significant scatter is observed both for the daytime BL and for the FT, though the correlation is generally better in the BL, where most of the modeled values are within a factor of 2 of the observations when the modeled and observed data are paired in both space and time. No obvious bias is observed for O_3 within the BL, though significant underpredictions are noted for O_3 in the FT. Also noticeable in these comparisons is the underprediction of modeled CO in the BL, which was also apparent in both the daytime and nighttime vertical profile comparisons for CO (at different locations) in Figure 3. *Wotawa and Trainer* [2000] attribute the widespread high CO concentrations observed over the eastern United States during the summer of 1995 to emissions associated with large forest fires in Canada. *McKeen et al.* [2002] further show that during the period of strongest fire influence, 10–30 ppb enhancements in O_3 levels through large regions of the eastern United States can be attributed to precursor species emitted as a result of these fires. The NO_x, CO, and hydrocarbon emission inventory used in these simulations does not account for such episodic events, so the CO underpredictions and the discrepancies in BL and FT O_3 can be attributed in part to the inadequate representation of this biomass burning source in the simulations.

[33] Also shown in Figure 4 are comparisons of space-time-paired mixing ratios for isoprene, HCHO, and H_2O_2. The ability of MAQSIP to accurately represent chemical transformations in the atmosphere depends upon reliable simulation of the free radical budgets. Carbonyl compounds, produced as a result of photo-oxidation of VOCs, are important in determining the free radical budgets in the atmosphere; they are a major source of free radicals through photolysis and also serve as a sink for available OH [e.g., *Trainer et al.*, 1987]. HCHO is produced as a result of OH-initiated oxidation of a variety of VOCs, while H_2O_2 is produced through radical termination reactions; thus comparing their modeled mixing ratios with observations provides an indirect measure of the model's ability to represent the photochemistry in an integrated sense. While significant scatter is noted in the modeled-observed correlations for these species, the model is able to capture the range of variability in the measured mixing ratios within the BL. The underprediction of highly reactive primary species such as isoprene in grid-based models can arise due to artificial dilution effects associated with instantaneous mixing of emissions over relatively large grid volumes and the consequent inadequate representation of its subsequent subgrid chemistry; underpredictions in isoprene concentrations will then translate to underprediction in its oxidation products, such as HCHO. The underprediction in modeled isoprene and HCHO could also arise due to uncertainty in isoprene emissions, which are currently estimated to be biased low [e.g., *Pierce et al.*, 1998]; the rate of production of HCHO from oxidation of anthropogenic VOCs is significantly smaller than that from isoprene. In a recent study, *Hanna et al.* [2005] estimated the uncertainties in isoprene emissions from BEIS3 and quantified their effect on O_3 predictions using three models, including MAQSIP. Their results suggest that the 95% confidence range on calculated uncertainties in isoprene emissions cover an order of magnitude. The resultant uncertainties in predicted ozone, however, were found to be only 15–20% across all models. Additionally, for each of the model grid cells, Hanna et al.

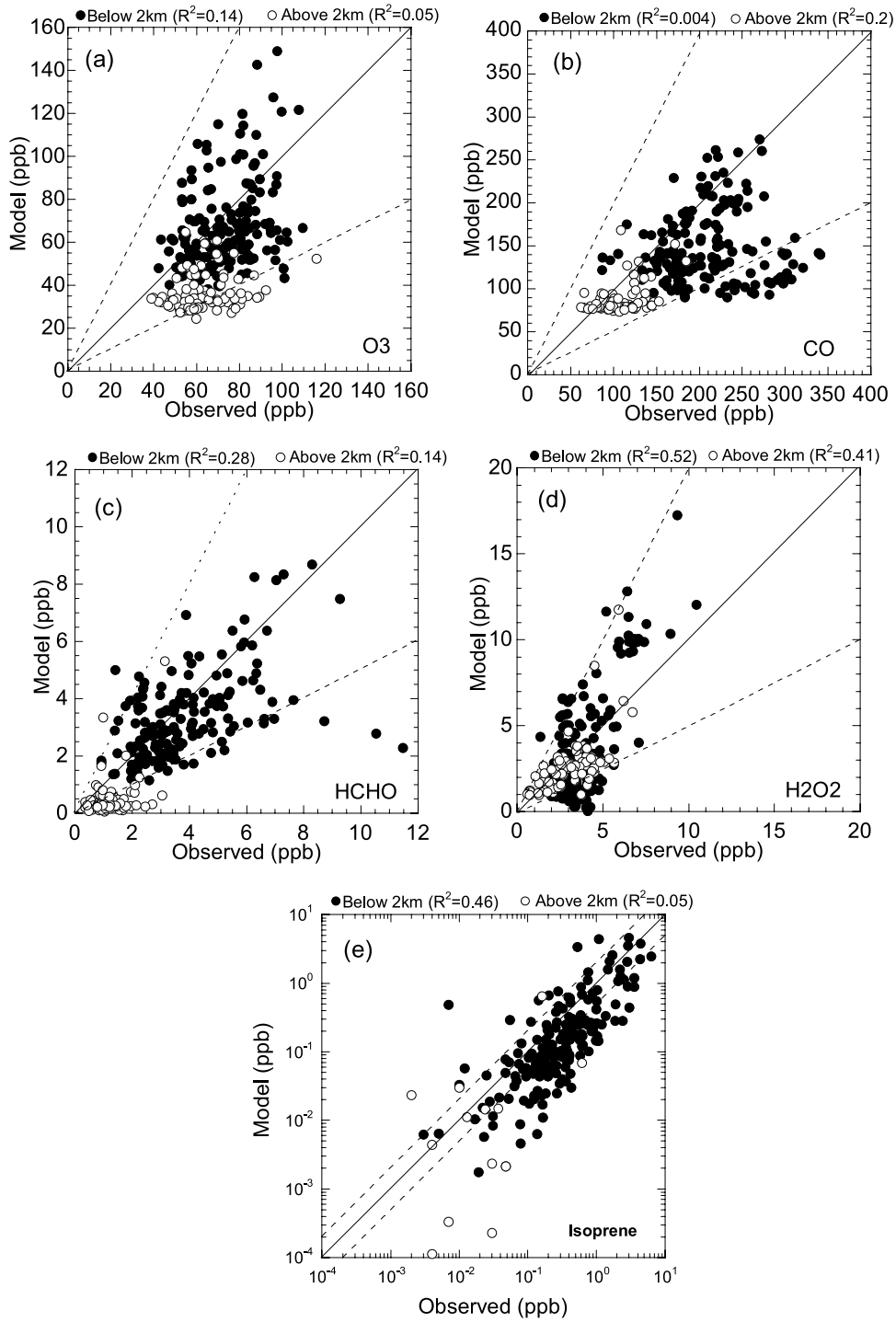

Figure 4. Correlation between model predictions and aircraft measurements for (a) O_3, (b) CO, (c) HCHO, (d) H_2O_2, and (e) isoprene. Filled circles correspond to data points in the daytime boundary layer (below 2 km altitude) while open circles represent data points in the free troposphere (above 2 km). Also shown are the 1:1 (solid) and 1:2 and 2:1 (dashed) lines.

did not find any significant correlation between variations in BEIS3 input parameters and variations in CTM-predicted O_3 concentrations. This suggests that over most of the eastern U.S., where O_3 production is NO_x-sensitive, the sensitivity of O_3 production to variations in isoprene emissions is likely to be small. Consequently, future corrections in the model bias for isoprene mixing ratios are not expected to systematically or adversely affect the model performance for surface O_3. The moderate correlation between the observed and modeled data depicted in Figure 4 also arises in part from comparing grid-averaged modeled values with point measurements [e.g., *Schere*, 1988]. *McKeen et al.* [1991] have noted that due to the variability in observations and the inability of coarse-resolution models to represent

subgrid-scale effects, moderate correlation between measured and predicted values is probably as good as can be expected. Another consistent feature noted in these correlations is the relatively large discrepancy (primarily underprediction) between modeled and observed FT values. This can be attributed to the initial and boundary conditions used in these model simulations, which were specified at typical background tropospheric values at all model heights. Consequently, model-predicted O_3 in the free troposphere is significantly lower (35–50 ppb) than measured values (50–90 ppb). These discrepancies highlight the need for improved model initialization and lateral boundary conditions in the FT, especially for long-term simulations wherein the representation of exchange processes between the FT and BL can influence predicted 3-D pollutant distributions.

[34] The model's ability to simulate the regionally averaged vertical profiles sampled by the aircraft campaigns during the study period is illustrated in Figure 5, which presents comparisons of the average composite vertical profiles for various species. In constructing these profiles, we averaged both the observed and the modeled data within each vertical model layer and over all the flights; the figure also shows standard deviation bars. These vertical profiles may thus be regarded as representing the mean conditions that occurred over middle Tennessee and surrounding areas during the study period. In general, the model tracks the composite average gradients within both the BL and FT for the various species, with some exceptions. Noticeable among these are the underpredictions for O_3 and HCHO in the FT and CO in the BL, as discussed earlier. These comparisons with regional aircraft data further highlight the important effect of model initialization and lateral boundary conditions on predicted FT distributions.

[35] The ability of the model to accurately represent chemical transformations in the atmosphere depends upon reliable simulation of the OH fields. As discussed earlier, HCHO is produced from OH-initiated oxidation of a variety of VOCs, and its rate of production due to OH oxidation of anthropogenic VOCs is significantly smaller than that from isoprene, due to a combination of low concentrations, slower kinetics, and smaller yields [e.g., *Carter and Atkinson*, 1996]. In their analysis of aircraft data, *Lee et al.* [1998] point out that at the concentrations measured during the study period, HCHO accounted for a substantial portion of the OH reactivity, comparable to that of isoprene and CO, and contributed up to 25–30% of the midday radical production. The comparisons of simulated HCHO mixing ratios with aircraft measurements in Figures 4 and 5 show that while the model tends to slightly underpredict HCHO, it simulates the range of variability in the measured mixing ratios within the boundary layer. To gain further insight into MAQSIP's ability to simulate radical chemistry over the study domain, we examined selected constituents in terms of their reactivity with OH. On the basis of the results of *Lee et al.* [1998], we limit our analysis to isoprene, HCHO, and CO, since their reactivity against OH was determined to dominate compared to the other OH sink species. Figure 6 elucidates the fractional contribution of the three constituents to the composite reactivity, defined as

$$\sum_i k_{OH_i}[R_i], \qquad (7)$$

where $[R_i]$ is the concentration of species i, k_{OH_i} is the rate constant for the reaction of species i with OH, and i = isoprene, CO, or HCHO. Within the daytime boundary layer (altitudes <2 km), the fractional contributions to the composite reactivity are reasonably well represented by the model. It is also interesting to contrast the variation of the fractional contribution of the individual constituents with the composite reactivity (right panels of Figure 6), with isoprene showing a reverse trend from that for CO and HCHO. At low reactivities, the relative contributions of CO and HCHO are higher, while at higher reactivities isoprene dominates the composite reactivity. This trend is seen in both the modeled values and the measurements and provides an indirect assessment of the model's ability to represent the spatial variability in the OH chemical sink.

4. Regional Particulate Matter Modeling

[36] The comprehensive gas-, aerosol-, and aqueous-phase species configuration of MAQSIP was used to simulate regional distributions of particulate matter (PM) and its composition over both the eastern and western United States. The eastern U.S. study focused on a summertime simulation (22–30 June 1996), while the western U.S. study focused on a winter period (14–20 January 1997); together they provide an assessment of the model predictions of PM over geographical domains characterized by differing emissions forcing as well as different meteorological conditions. For both cases a three-day model spin-up was used prior to the period of interest. Further, both cases used a 36-km horizontal grid resolution for the model simulations, 23 vertical layers from the surface up to 100 mb, input meteorological data derived from MM5 simulations, and emissions data based on the 1996 National Emissions Inventory (NEI). Model predictions of fine particulate matter ($PM_{2.5}$) and its compositional characteristics were evaluated against measurements from two regional networks, the IMPROVE network, which reports two 24-hour samples each week, and the Clean Air Status and Trends Network (CASTNET) (http://www.epa.gov/castnet), which reports weekly measurements. Measurements from IMPROVE were averaged over each period of interest. Given their relatively lower temporal frequency, measurements from CASTNET for June 1996 and January 1997 were used to create representative monthly averages for the respective periods.

[37] Figures 7 and 8 present comparisons of event-averaged model predictions (over the periods 22–30 June 1996 and 14–20 January 1997, respectively) against these averaged measurements for the two cases. Figures 7a and 8a show the predicted surface-layer, event-averaged concentrations of the total $PM_{2.5}$, which includes the fine aerosol species mentioned in section 2.5. These regional spatial distributions of predicted concentrations arise from both primary emissions and secondary aerosol formation downwind of the major source regions. Figures 7b and 8b show comparisons of these predictions (at model grid cells corresponding to the locations of measurement sites) against measurements from the IMPROVE network. In general, the model captures the spatial variability in the measured $PM_{2.5}$ concentrations (r^2 = 0.5), though there is considerable scatter in the correlations and a tendency to overpredict in the western U.S. winter case.

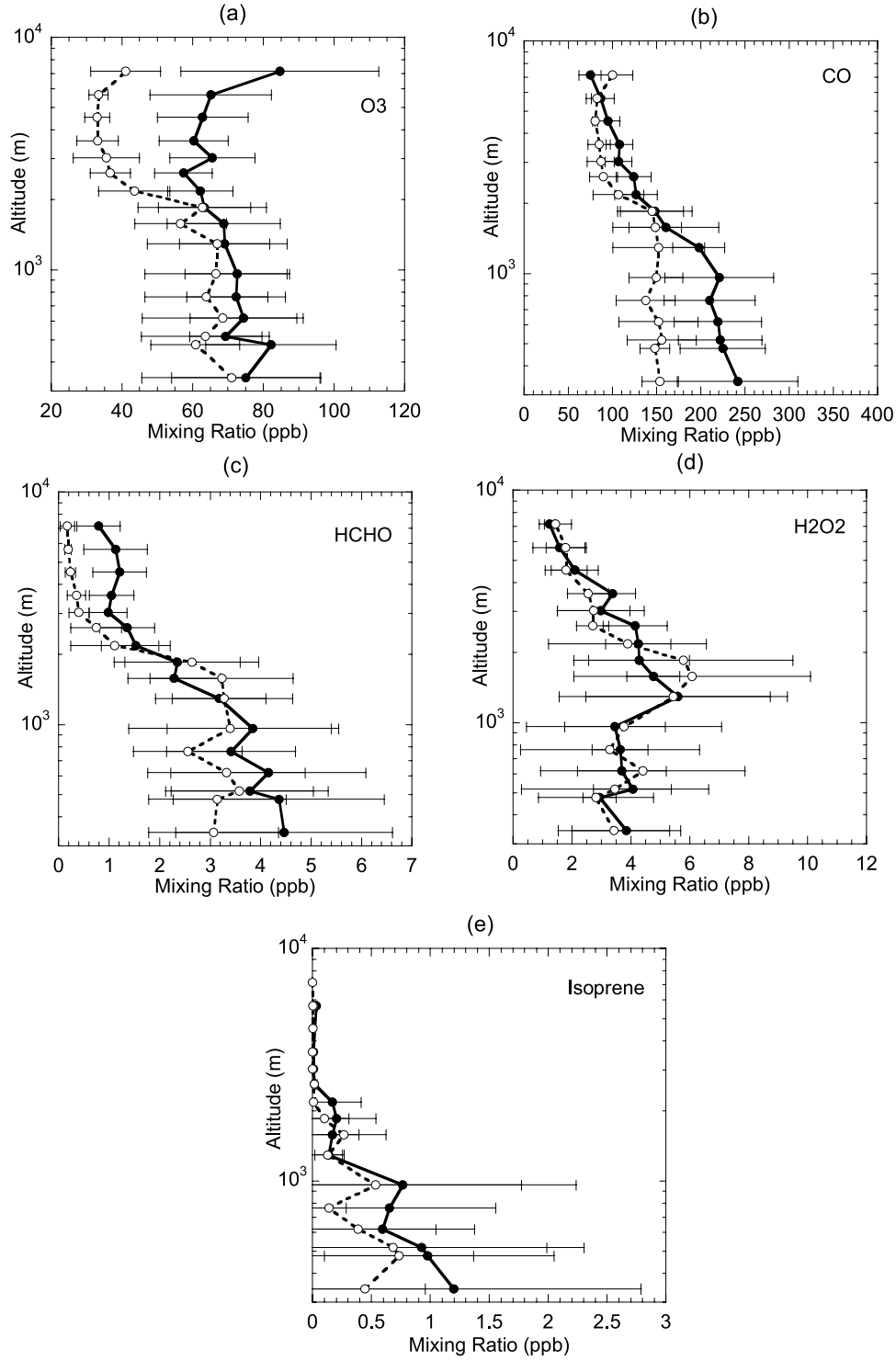

Figure 5. Comparison of regionally representative, average vertical distributions of various species (including standard deviation bars) during June–July 1995, based on spatially and temporally paired modeled (dashed line) and measured (solid line) data: (a) O_3, (b) CO, (c) HCHO, (d) H_2O_2, and (e) isoprene.

[38] Figures 7c and 7d and 8c and 8d compare the predicted compositional characteristics of the inorganic fine particulates against measured values. Figures 7c and 8c address particulate sulfate, nitrate, and ammonium concentrations; CASTNET reports measurements for SO_4^{2-}, NO_3^-, and NH_4^+, while IMPROVE reports SO_4^{2-} and NO_3^-. Both the measurements and the model show that in the eastern United States, SO_4^{2-} is a relatively large fraction of the $PM_{2.5}$ mass, due both to the presence of numerous emission sources downwind of the Ohio Valley and to

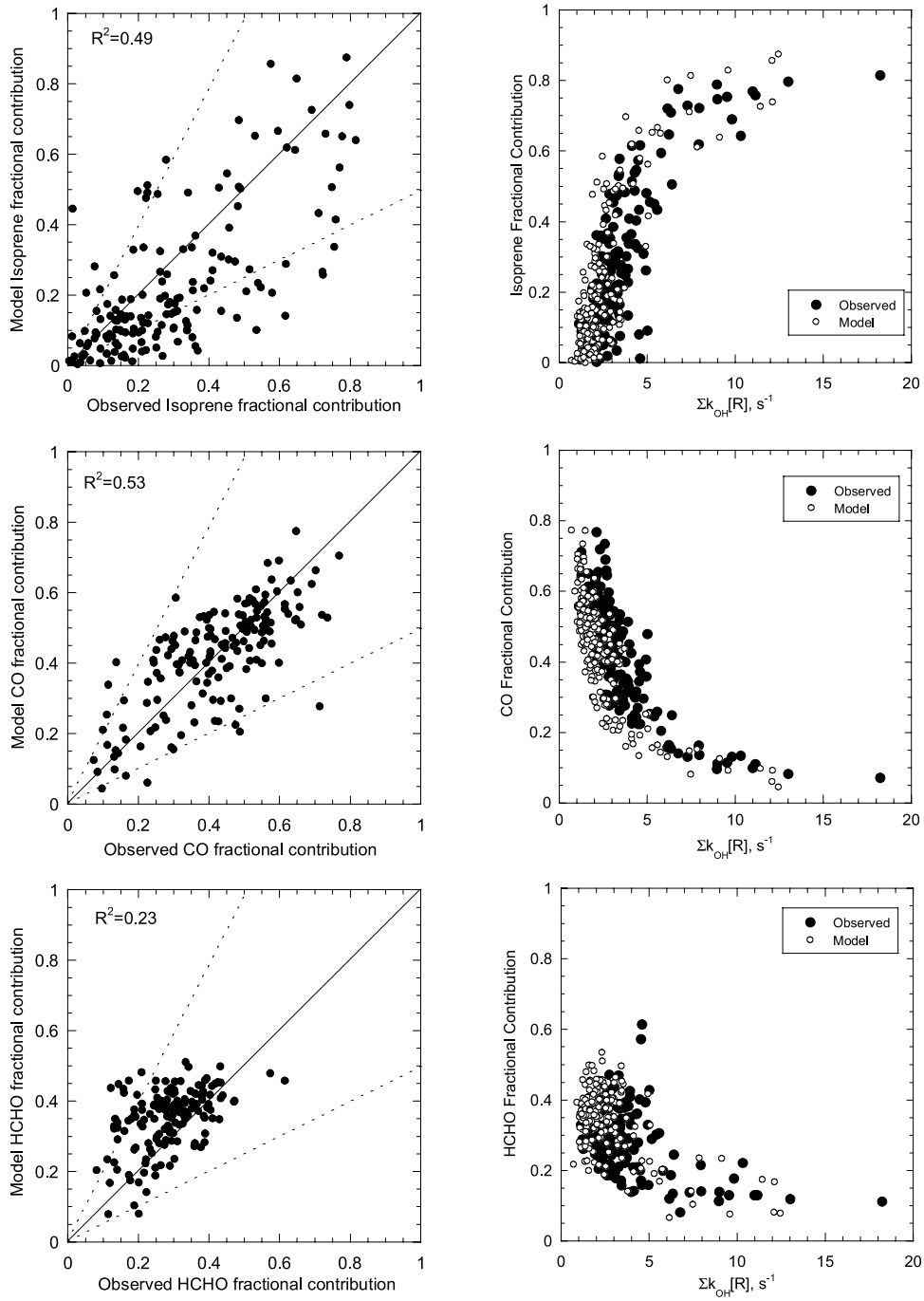

Figure 6. Modeled and measured fractional contributions of isoprene, CO, and HCHO to the composite reactivity at altitudes <2 km: scatter plots of modeled versus observed fractional contributions (left) and correlation between individual fractional contributions and composite reactivity (right). Also shown in the left panels are the 1:1 (solid) and 1:2 and 2:1 (dashed) lines.

the predominance of convective activity in the summertime in this region. Further, particulate nitrate formation is suppressed in these simulations due to the temperature dependence of the phase partitioning of nitrate; higher temperatures lead to more nitrate partitioning to the gas phase as HNO_3. In contrast, in the western United States in winter, particulate nitrate is a significant fraction mainly due to the lower temperatures, and also the relatively low concentrations of SO_2 needed for sulfate formation compared to the eastern U.S.; these aspects of the measurements are captured in the simulations (Figure 8c). Also in the eastern U.S. summer case, while the SO_4^{2-} and NH_4^+ concentrations are moderately underpredicted, the model captures the relative compositional characteristics of SO_4^{2-}, NO_3^-, and NH_4^+ in the inorganic PM mass reasonably well (Figure 7c). In the western U.S. winter case, the model tends to overpredict concentrations of all three components relative to the observations (Figure 8c). The overpredictions

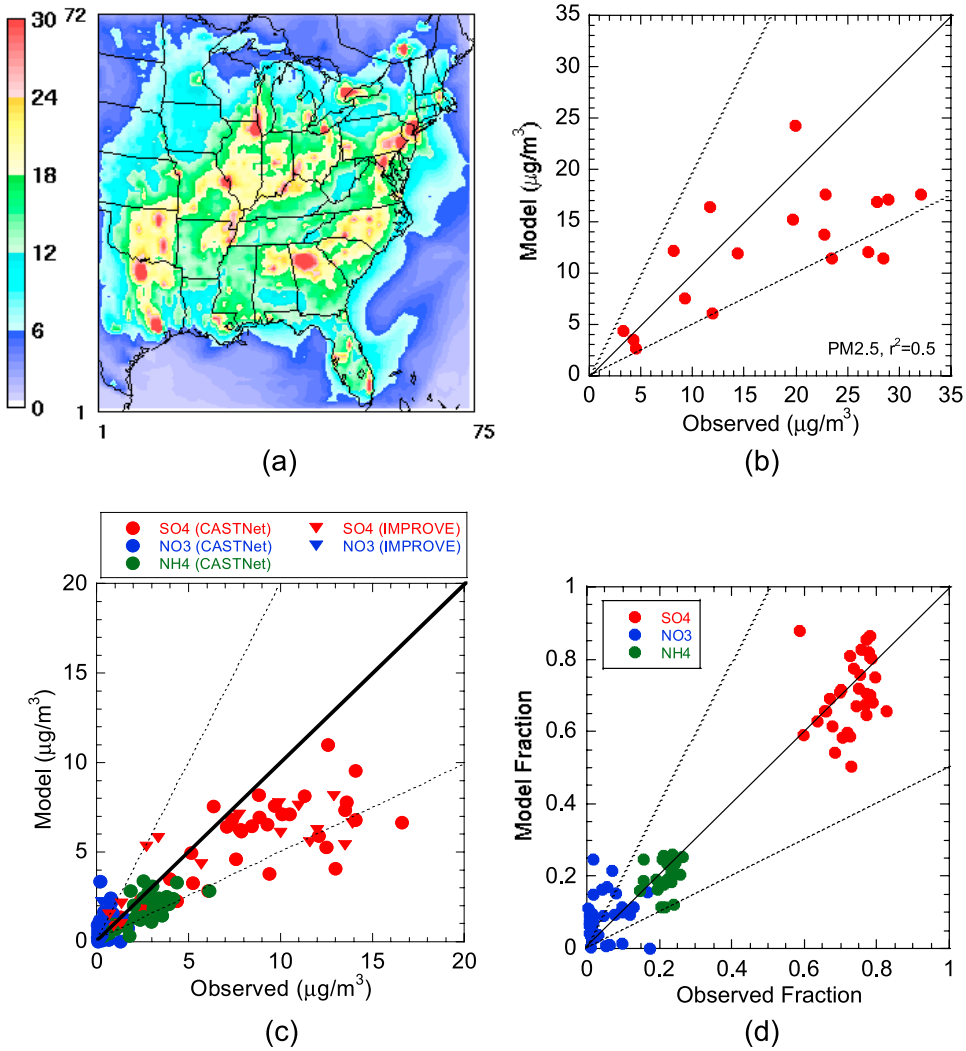

Figure 7. Fine particulate mass and compositional characteristics over the eastern U.S. for a summer case during June 1996: (a) modeled spatial distribution of average $PM_{2.5}$ concentrations in the lowest model layer; (b) comparison of modeled $PM_{2.5}$ concentrations with IMPROVE measurements; (c) comparison of modeled SO_4^{2-}, NO_3^-, and NH_4^+ concentrations with IMPROVE and CASTNET measurements; (d) comparison of modeled SO_4^{2-}, NO_3^-, and NH_4^+ fractions in the inorganic $PM_{2.5}$ with CASTNET measurements. Also shown in the scatter plots are the 1:1 (solid) and 1:2 and 2:1 (dashed) lines.

in NO_3^- and NH_4^+ in the western U.S. winter case arise in part from uncertainty in seasonal allocation of annual NH_3 emission inventories, especially during the cooler months when NH_3 emissions are quite low [e.g., *Mathur and Dennis*, 2003]. For conditions typical of the eastern United States, *Gilliland et al.* [2003], for instance, estimate scaling down annual NH_3 emissions from the NEI by as much as 68% for wintertime conditions, based on their model inversion analysis. These overpredictions could also be related in part to uncertainties associated with HNO_3 production via heterogeneous pathways and its effects on simulated airborne total nitrate. Recent studies [e.g., *Riemer et al.*, 2003] suggest that simple parameterizations typically employed in 3-D models may overestimate the effects of this pathway on simulated photochemistry; overestimation of nitrate formation through this pathway contributes to an overestimation of particulate nitrate, which is further magnified in NH_3-rich regions, especially in winter, since wintertime NH_3 emissions are overestimated in the inventory. However, in assessing the magnitude of the bias in the model relative to the measurements it is also important to consider the bias intrinsic in the measurements themselves. For instance, *Sickles* [1999] reports that CASTNET NH_4^+ values may be biased high due to capture and retention of NH_3 by acidic sites on particles collected by the filter. Recently, *Ames and Malm* [2001] compared particulate SO_4^{2-} and NO_3^- concentrations from the IMPROVE and CASTNET networks to quantify the relative bias between the two networks. They found that in the west and the interior desert/mountain regions the NO_3^- values reported by CASTNET were higher than those from the IMPROVE network, while the trend was opposite at the limited comparison sites in the eastern United States. Particulate NO_3^- loss in the measurements due to temperature-

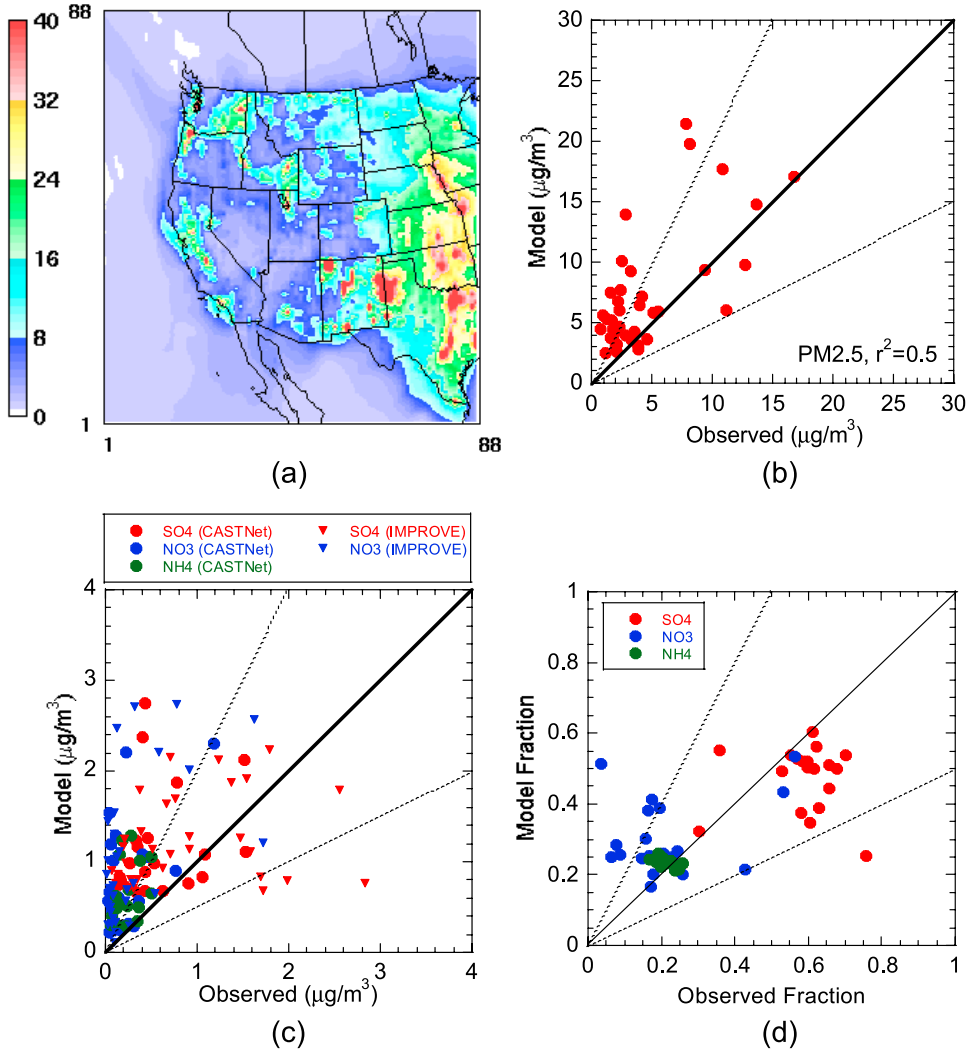

Figure 8. Same as Figure 7, but for a winter case during January 1997 over the western U.S.

dependent volatilization can result in such bias [e.g., *Benner et al.*, 1991] and also contribute to the modeled NO_3^- overpredictions. Another mechanism causing the difference in particle NO_3^- concentrations between the two networks could be the enhanced coarse-particle NO_3^- collection efficiency in the non-size-selective CASTNET sampler. However, these two mechanisms result in observational biases that are opposite in direction [*Ames and Malm*, 2001], thus making it difficult to develop a universal "correction factor" to facilitate a quantitative assessment of model bias. It is also possible that the comparisons between modeled values and observations are influenced by a systematic bias in a model process (e.g., mixing height and intensity of mixing) that impacts all aerosol components in a similar manner. For instance, the boundary layer heights used in the western U.S. winter case were found to be poorly predicted by the meteorological model and often too low; this contributes to the systematic high bias noted for all PM components in Figure 8c. Further, the metastable assumption may not represent the aerosol state under the relatively dry conditions prevalent in many parts of the western U.S.

[39] To reduce such biases intrinsic in both the measurements and the model, we compared the predicted relative fractions of these three primary inorganic PM components against measured fractions based on the CASTNET data (Figures 7d and 8d). Compared to the absolute concentration levels, the model does better at capturing the fractions of the three inorganic components relative to the total inorganic (dry) mass and also their spatial variability. The better agreement of model predictions of the relative fractions of SO_4^{2-}, NO_3^-, and NH_4^+ compared to those of their individual concentrations suggests that the model chemistry and its processing of emissions capture the speciation of the inorganic aerosol mass adequately, although it is likely that systematic biases may exist in a model process (e.g., mixing) or in the input emissions.

5. Visibility Modeling and Analysis

[40] To illustrate MAQSIP's capability to assist in analyzing atmospheric visibility, model estimates for visibility parameters are presented for the eastern U.S. summer case and the western U.S. winter case discussed in the previous section. Figures 9a and 9b present event-averaged regional visibility estimated using the IMPROVE empirical algorithm [*Sisler and Malm*, 2000] and the Mie algorithm

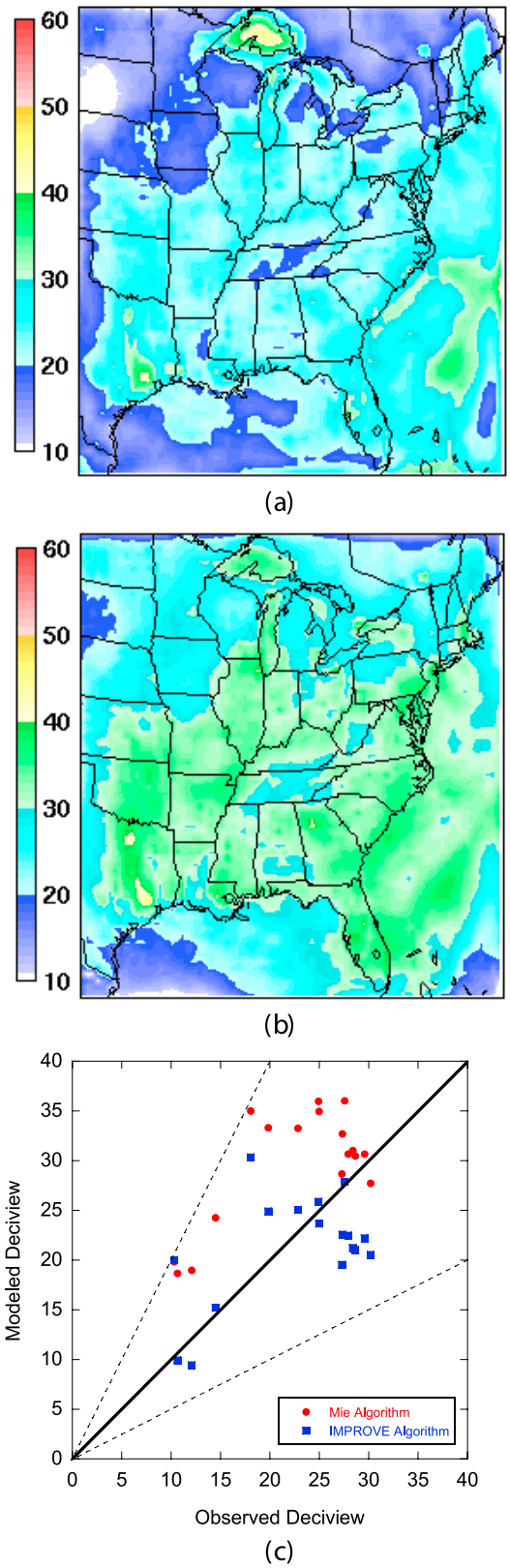

Figure 9. Modeled and observed deciview over the eastern U.S. during June 1996: (a) modeled distributions based on IMPROVE empirical algorithm; (b) modeled distributions based on Mie algorithm; (c) comparison of modeled values in Figures 9a and 9b with measurements. Also shown are the 1:1 (solid) and 1:2 and 2:1 (dashed) lines.

[*Wiscombe*, 1980], respectively, for the eastern U.S. summer case, while Figures 10a and 10b show analogous panels for the western U.S. winter case. Comparisons of modeled and observed estimates of deciview at the IMPROVE monitoring sites for the respective cases are shown in Figures 9c and 10c.

[41] For both regions simulated, the Mie algorithm estimates higher deciviews than the IMPROVE empirical method. Further, the Mie-based results are biased high relative to the observed values. This may indicate that MAQSIP predicts mass concentrations better than size distribution parameters such as number concentration and aerosol effective radius; however, this cannot be verified, as detailed regional measurements of aerosol size parameters are currently lacking. Another possible source of discrepancy between the Mie and the empirically based visibility estimates could be the specification of the aerosol refractive index used in the Mie calculations. Since the refractive index is parameterized on aerosol liquid water content (LWC), it is possible that in some situations it is not representative of the modeled aerosol chemical composition. In contrast, the IMPROVE visibility estimate is based on the mass-based scattering efficiencies of the different aerosol constituents and may thus provide better agreement with observed visibility in situations where aerosol size parameters are not adequately simulated. It is also possible that the observed overprediction of the hygroscopic aerosol species in the west (Figure 8c) could result in a possible overprediction of the aerosol LWC, which would yield higher scattering efficiencies than observed.

[42] Figure 11 illustrates the correlation between modeled and observed fractional contributions of various aerosol constituents to the aerosol extinction as calculated by the empirical algorithm. While there is significant scatter, it occurs primarily for components that have relatively small contributions (typically below 10%) to the estimated visibility; most of the data points for components that contribute >10% exhibit significantly less scatter and are generally within a factor of 2 of the observations. For the eastern U.S. summer case, both the modeled and observed data show that SO_4^{2-} contributes the largest fraction (35–85%), while organic mass contributes up to 20–25%. In contrast, for the winter conditions simulated in the west, SO_4^{2-} and NO_3^- each contribute comparable amounts (20–50%) to the light extinction, due to lower SO_4^{2-} and higher NO_3^- concentrations relative to the east. In the western U.S. study, overprediction in NO_3^- mass (Figure 8c) results in overprediction of its contribution to light extinction. The overprediction of the fine soil contribution combined with the underprediction of the coarse mass contribution suggests that the fractions of fugitive dust emissions apportioned to the fine and coarse modes need further evaluation. Further, the emissions model does not include windblown dust, a significant component of coarse dust that is missing in these simulations.

6. Nested Grid Applications and Effects of Grid Resolution

[43] Since the dynamical and chemical processes leading to air pollution occur on a wide range of spatial scales, accuracy of model results is closely related to the resolution

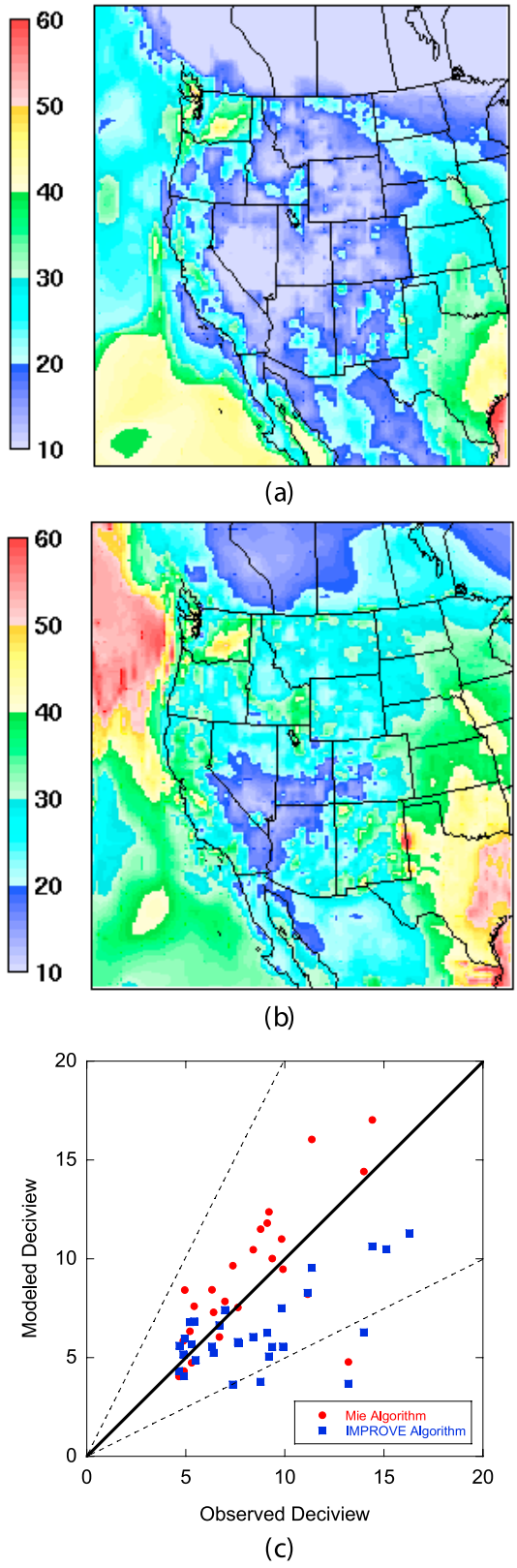

Figure 10. Same as Figure 9, but for a winter case during January 1997 over the western U.S.

of the computational mesh on which model calculations are performed; the interactions among atmospheric processes regulating the fate of atmospheric pollutants must be effectively resolved [e.g., *Odman and Russell*, 1991; *Mathur et al.*, 1992]. *Sillman et al.* [1990] suggest that degrading the model horizontal resolution can cause a systematic positive bias in O_3 simulation, since the artificial dilution of NO_x emissions over relatively large grid volumes can increase the O_3 production efficiency per unit of NO_x oxidized [*Liu et al.*, 1987]. Similar positive bias in predicted O_3 resulting

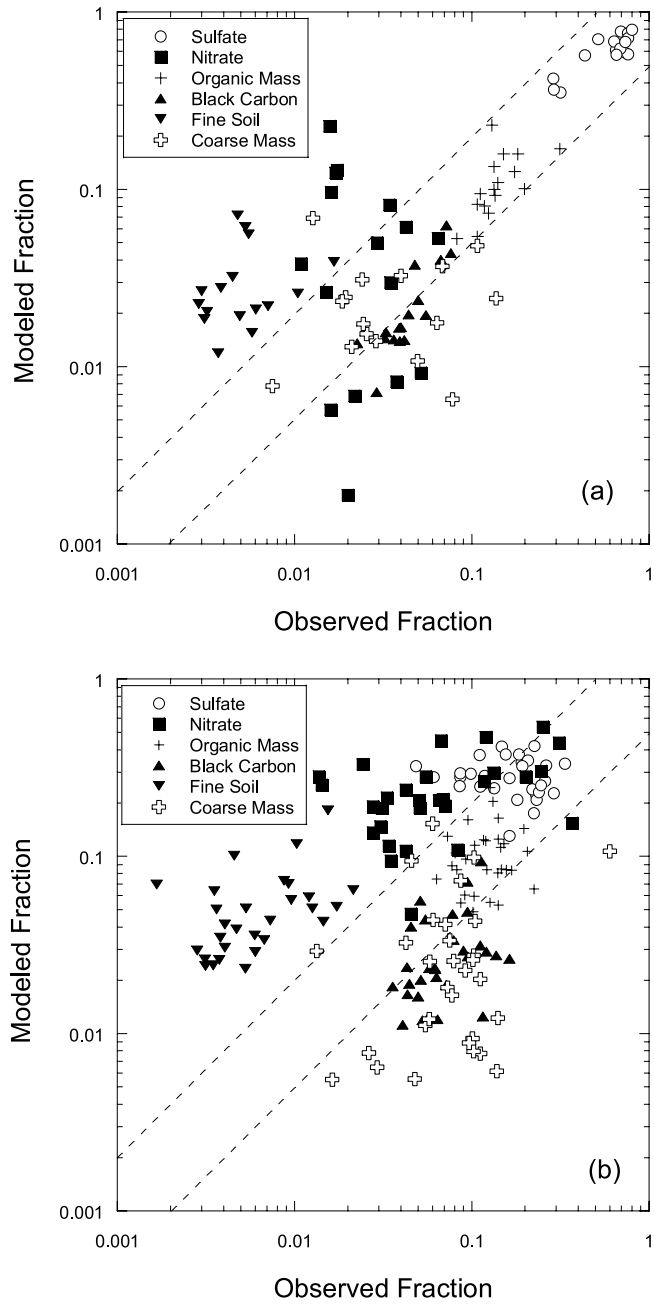

Figure 11. Comparison of modeled and observed fractional contributions of various aerosol constituents to aerosol extinction: (a) for June 1996 over the eastern U.S.; (b) for January 1997 over the western U.S. Dashed lines represent the 1:2 and 2:1 lines.

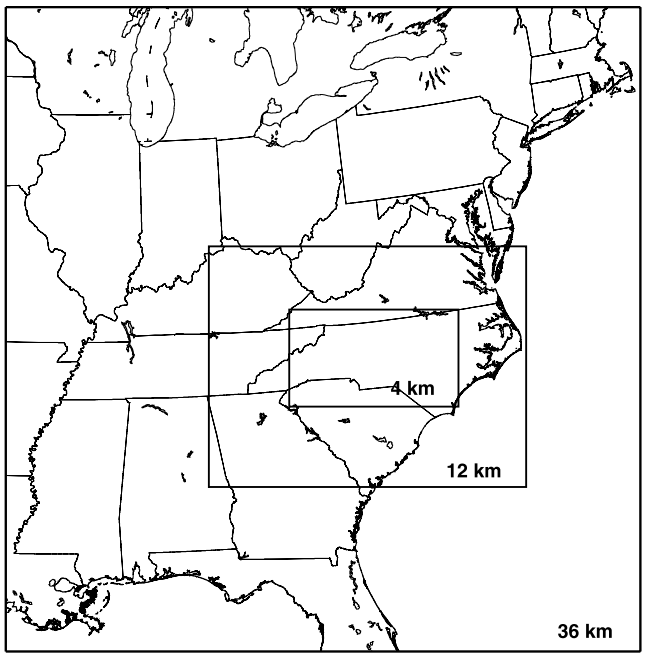

Figure 12. Model domain and the 36-, 12-, and 4-km nested-grid configuration for the North Carolina ozone simulation.

from degradation of horizontal grid resolution has also been reported in simulations over southern California by *Kumar et al.* [1994]. Through box-model calculations of O_3 production efficiency for a variety of conditions, *Liang and Jacobson* [2000] suggest that coarsely resolved models might underpredict or overpredict O_3 production because they are unable to accurately represent the blending of air masses of different origin.

[44] MAQSIP was used to simulate O_3 distributions over North Carolina for 19–25 June 1996. The period of 21–24 June was characterized by elevated O_3 levels that were associated with a frontal system to the north and a high-pressure system to the southwest of the state. The movement of the front resulted in recirculation during this period. Figure 12 illustrates the nested-grid configuration employed: a 36-km-resolution outer grid over the eastern U.S., a nested 12-km grid over the southeastern U.S., and a 4-km grid covering portions of North Carolina including the metropolitan areas of Charlotte, Raleigh-Durham-Chapel Hill, and Greensboro-Winston Salem. The vertical extent ranging from the surface to 100 mb was discretized using 26 layers of variable thickness, with a 38-m lowest-layer thickness and nine layers within the first 1 km. Meteorological fields were derived from MM5 simulations using a one-way nesting with the same 36-, 12-, and 4-km grid configuration as for MAQSIP. Temperature-dependent (e.g., biogenic emissions) and stability-dependent (e.g., plume rise for point sources) emission rates for each grid cell were based on meteorological information for each grid system.

[45] To illustrate the effects of grid resolution on simulated O_3 spatial distributions and temporal trends, we limit our analysis to the spatial extent of the 4-km-resolution domain, which is common to all three grid systems. Since the simulations employed one-way nesting, we can systematically study the effects of artificial dilution and representation of land surface characteristics resulting from improved horizontal resolution on simulated O_3 distributions. Figure 13 presents the spatial distributions of simulated surface-level O_3 from each of the three grid resolutions at 1900 UTC 24 June 1996. Overlaid on the simulated distributions are the observed O_3 values at AIRS stations within the region. Comparing these observations with the simulated distributions shows that refining the grid resolution from 36 km to 4 km significantly affects the simulated O_3 distributions, with the 4-km grid providing a better representation of the spatial gradients in surface O_3. Also noticeable in these comparisons is the overprediction of O_3 at the 36-km and 12-km resolutions, resulting from a wider O_3 plume along the transportation corridor between the Charlotte and Greensboro areas. At the 4-km resolution this is rectified; the simulated O_3 plume is much narrower.

[46] Figure 14 compares the temporal evolution of the simulated hourly ozone at the three resolutions with measured data at selected sites. The Arrowood and Duke Street sites represent urban locations, while Bethany, Hattie Ave-

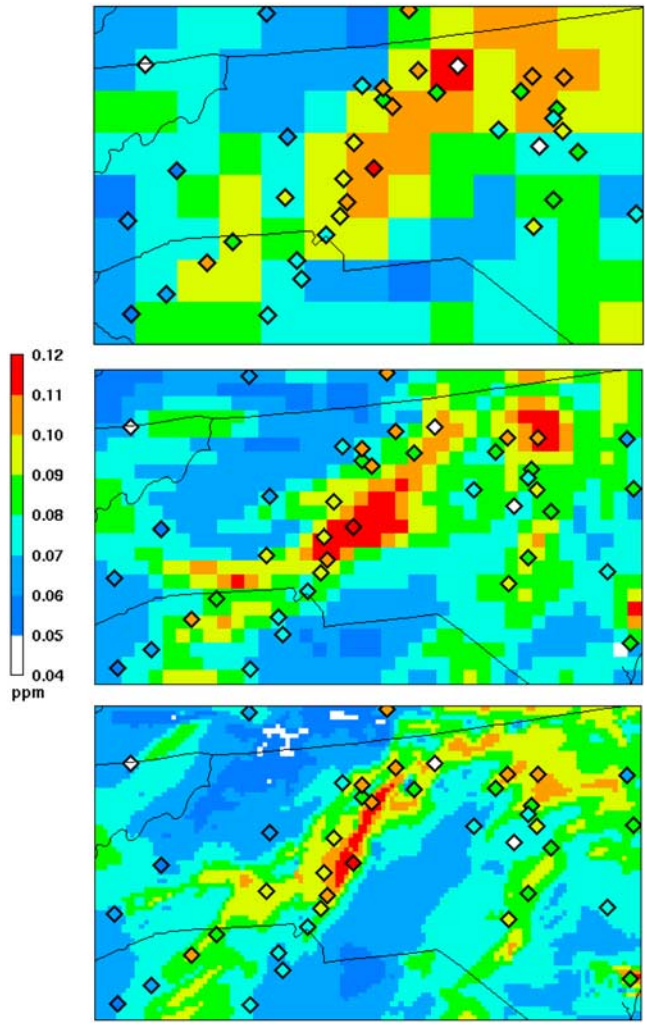

Figure 13. Simulated surface O_3 distributions over North Carolina at 1900 UTC 24 June 1996, using (a) 36-km, (b) 12-km, and (c) 4-km grid resolutions. The color-coded diamonds represent corresponding AIRS ozone measurements.

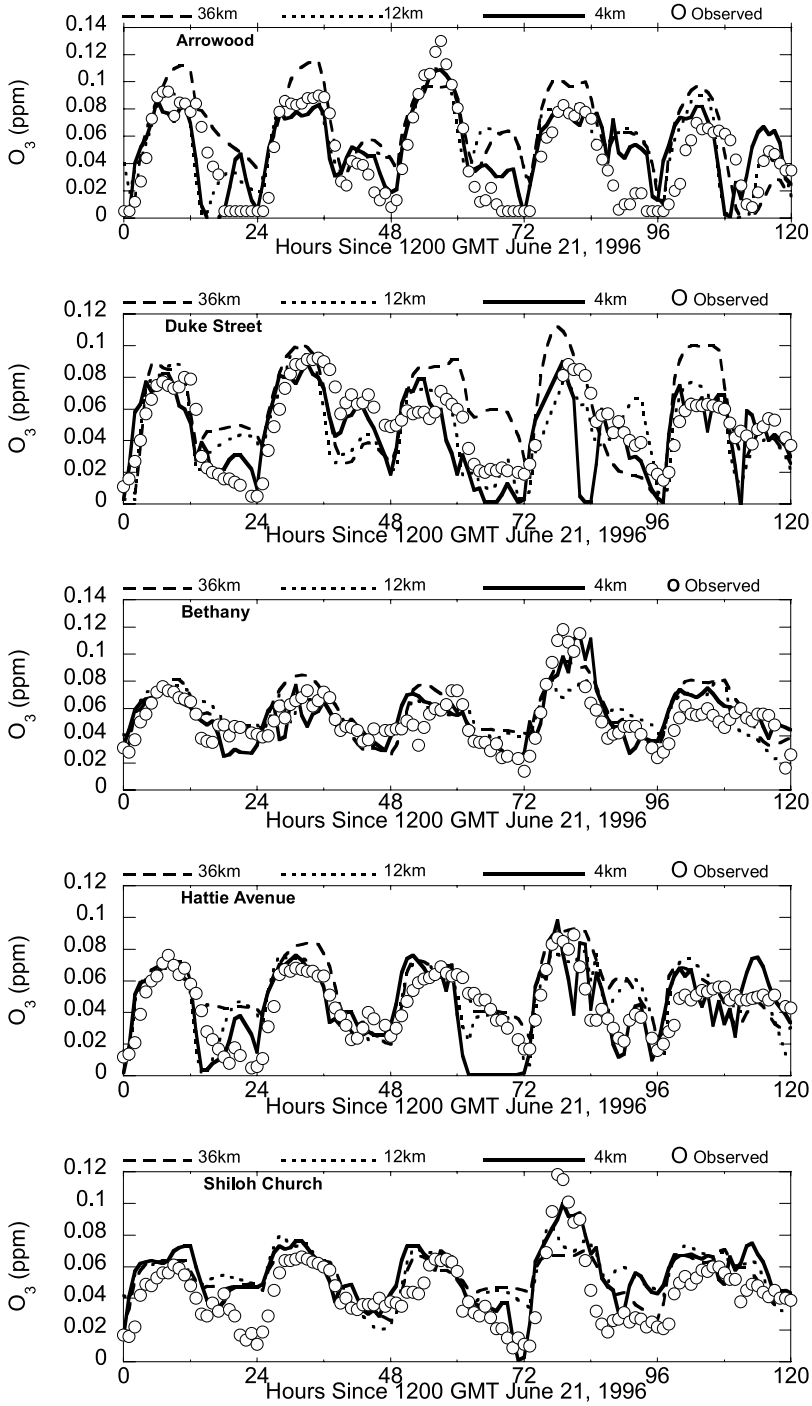

Figure 14. Comparison of temporal variations in surface O_3 simulated by the 36-km, 12-km, and 4-km grids with observations at selected sites: Arrowood (35.113°N, 80.919°W), Duke Street (35.035°N, 78.904°W), Bethany (36.308°N, 79.858°W), Hattie Avenue (36.11°N, 80.226°W), and Shiloh Church (36.203°N, 80.215°W).

nue, and Shiloh Church are downwind of major point sources. Noticeable in these comparisons is the overprediction of peak O_3 at the urban locations at the 36-km resolution, resulting from higher O_3 production efficiency per unit NO_x oxidized relative to the 12- and 4-km grids, as discussed earlier. Additionally, improving the resolution from 36 km to 4 km systematically helps reduce the nighttime O_3 overprediction at these urban locations due to improved representation of the O_3 titration by NO_x emissions. Comparisons at the three other sites in Figure 14, which are frequently impacted by plumes from point sources, illustrate that the 4-km grid provides the most realistic O_3 simulation, due to better representation of the downwind lateral dispersion of emissions and their chemical

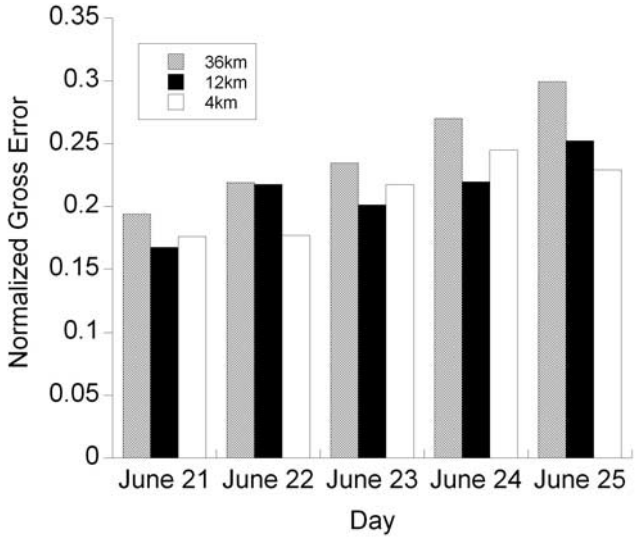

Figure 15. Normalized gross error in simulated surface O_3 for the 36-km, 12-km, and 4-km grids.

evolution; the 36-km simulation tends to overpredict daytime values, while both over- and underpredictions are noted for the 12-km simulation.

[47] Quantitative estimates of error in modeled surface O_3 relative to the measurements for the three grid resolutions for each simulation day are presented in Figure 15; the statistic used is normalized gross error (NGE), as defined in equation (6). For each simulation day, the largest NGE values are noted for the 36-km grid. Refining the grid resolution to 12 km and 4 km reduces NGE, though the improvements in model error are modest when examined globally as in Figure 15.

7. Summary and Concluding Remarks

[48] In its current form, MAQSIP has been applied to a variety of problems to study the distribution of tropospheric O_3, particulate matter, and airborne acids over a variety of domains and over temporal scales ranging from episodic to seasonal. The statistical correlations between simulated surface O_3 concentrations and measurements on a daily and episodic basis are comparable to those obtained with other models [e.g., *Hogrefe et al.*, 2001a, 2001b; *Fiore et al.*, 2003]. The daily performance metrics are found to be within the suggested performance criteria for management evaluation studies. Analyses of predicted surface O_3 concentrations over an entire summer season indicate that the model captures the day-to-day variations in regional O_3 distributions, and the dynamic range of the observations on a seasonal basis [*Kasibhatla and Chameides*, 2000]; it also represents the diurnal, synoptic, and longer-term timescales better than the intraday component [*Hogrefe et al.*, 2001b]. These results demonstrate the model's viability for use in longer-term simulations of surface O_3 trends and distributions. However, such longer-term simulations also warrant further improvements in the model, especially in its representation of processes in the free troposphere and its exchange with the boundary layer. Comparisons with limited observational aircraft data show moderate to poor correlation with measurements in the free troposphere. While these discrepancies can be attributed in part to model initialization and lateral boundary conditions specification, further evaluation of the chemical mechanisms currently used in the model for representing chemistry in the free troposphere is needed. Another area of potential improvement would be the incorporation of emissions due to lightning and to episodic biomass burning and forest fires, which are not accounted for in most regional models.

[49] The limited comparisons with available speciated PM measurements show that while the model can represent the spatial variability of the total fine particulate matter ($PM_{2.5}$) mass and its relative partitioning among the primary inorganic components (SO_4^{2-}, NO_3^-, NH_4^+) over both the eastern and western United States, the predictions for the individual components are biased high over the west in the winter. The magnitude of this model bias, however, cannot be accurately estimated given the intrinsic bias in the currently available measurements. Emissions of both wintertime ammonia and NO_x plus uncertainties in current representation of heterogeneous pathways for nitrate formation, combined with the poorly predicted boundary layer heights used by the model, may be responsible for this high model bias. Further, while MAQSIP includes a detailed treatment of aerosol dynamics, regional measurements are currently insufficient to directly evaluate the estimated aerosol size distributions. Nevertheless, the availability of aerosol size and number distributions in the predictions facilitates the use of the model in exploring potential radiative and optical effects of tropospheric aerosol loading, and provides expanded capability for use of the model in addressing evolving issues related to regional visibility impairment and climate perturbations [*Mathur et al.*, 2000] (also see http://www.cep.unc.edu/empd/projects/integrated/index.shtml).

[50] The results presented in this paper, based on a few selected MAQSIP applications, provide an initial assessment of the model's performance and capabilities. A number of modeling studies with MAQSIP are currently underway and will provide further assessments of the adequacies and inadequacies of the various modeled processes and further contribute to its evaluation. Unlike numerical weather prediction, which involves multiple runs of multiple models, atmospheric chemistry and transport modeling has not been able to benefit from the repeated forecast applications that test a model's ability to reliably predict the distribution of trace species under various conditions. Guided by the performance of the model over a full season of active photochemistry, a quasi-operational real-time atmospheric chemical forecast system that couples the MM5 and an optimized version of MAQSIP with the emissions processing model SMOKE has also been developed [*McHenry et al.*, 2004]; the system has been operational since 1999. Continuous analyses of such repeated forecast applications provide unique opportunities to test the model under various dynamical and chemical conditions and will help further improve the model.

[51] **Acknowledgments.** The development of MAQSIP was initiated under cooperative agreements CR822066, CR822053, CR822059, and CR823634 with the U.S. Environmental Protection Agency (EPA). Further development, refinement, application, and evaluation of the model was made possible due in part to funding through research grants and contracts

NAGW-4701 (NASA), 9711488 (NSF), GR826773 (EPA), EA8009 (SESARM), and EA02012 (NCDENR). The support from these is gratefully acknowledged. Contributions by P. Kasibhatla, W. L. Chameides, and S. T. Rao in analysis and interpretation of model results through various collaborations are also gratefully acknowledged. We are thankful to Z. Adelman, E. Adams, M. Houyoux, and J. Vukovich for their assistance with input data preparation and model testing. We thank the NOAA Aeronomy Laboratory's Tropospheric Chemistry Division for providing processed aircraft data and S. McKeen and T. Ryerson for helpful discussions on these data. Additional measurement data used in this study were obtained from the AIRS, CASTNET, and IMPROVE networks and the SOS and NARSTO databases. The research presented here was performed under the Memorandum of Understanding between the U.S. Environmental Protection Agency (EPA) and the U.S. Department of Commerce's National Oceanic and Atmospheric Administration (NOAA) and under agreement number DW13921548. Although it has been reviewed by EPA and NOAA and approved for publication, it does not necessarily reflect their policies or views.

References

Alapaty, K., and R. Mathur (1998), Effects of atmospheric boundary layer mixing representations on vertical distribution of passive and reactive tracers, *Meteorol. Atmos. Phys.*, *69*, 101–118.

Ames, R. B., and W. C. Malm (2001), Comparison of sulfate and nitrate particle mass concentrations measured by IMPROVE and the CDN, *Atmos. Environ.*, *35*, 905–916.

Benner, C. L., D. J. Eatough, N. L. Eatough, and P. Bhardwaja (1991), Comparison of annular denuder and filter pack collection of HNO_3(g), HNO_2(g), SO_2(g), and particulate nitrate, nitrite and sulfate in the south west desert, *Atmos. Environ.*, *25A*, 1537–1545.

Binkowski, F. (1999), Aerosols in Models-3 CMAQ, in *Science Algorithms of the EPA Models-3 Community Multiscale Air Quality (CMAQ) Modeling System*, *EPA/600/R-99/030*, edited by D. Byun and J. Ching, pp. 10-1–10-24, chap. 10, Off. of Res. and Dev., U. S. Environ. Prot. Agency, Washington, D.C.

Binkowski, F. S., and U. Shankar (1994), Development of an algorithm for the interaction of a distribution of aerosol particles with cloud water for use in a three-dimensional Eulerian air quality model, paper presented at Fourth International Aerosol Conference, Am. Assoc. for Aerosol Res., Cincinnati, Ohio.

Binkowski, F. S., and U. Shankar (1995), The Regional Particulate Matter Model: 1. Model description and preliminary results, *J. Geophys. Res.*, *100*, 26,191–26,209.

Blackadar, A. K. (1976), Modeling the nocturnal boundary layer, paper presented at Third Symposium on Atmospheric Turbulence, Diffusion and Air Quality, Am. Meteorol. Soc., Raleigh, N.C.

Bott, A. (1989a), A positive definite advection scheme obtained by nonlinear renormalization of the advective fluxes, *Mon. Weather Rev.*, *117*, 1006–1015.

Bott, A. (1989b), Reply, *Mon. Weather Rev.*, *117*, 2633–2636.

Byun, D. W., and J. K. S. Ching (Eds.) (1999), Science algorithms of the EPA Models-3 Community Multiscale Air Quality (CMAQ) modeling system, *Rep. EPA/600/R-99/030*, Off. of Res. and Dev., U.S. Environ. Prot. Agency, Washington, D.C.

Byun, D. W., J. Young, J. Pleim, M. T. Odman, and K. Alapaty (1999), Numerical transport algorithms for the Community Multiscale Air Quality (CMAQ) chemical transport model in generalized coordinates, in *Science Algorithms of the EPA Models-3 Community Multiscale Air Quality (CMAQ) Modeling System*, *EPA/600/R-99/030*, edited by D. Byun and J. Ching, pp. 7-1–7-56, Off. of Res. and Dev., U. S. Environ. Prot. Agency, Washington, D.C.

Carmichael, G. R., L. K. Peters, and R. D. Saylor (1991), The STEM-II regional-scale acid deposition and photochemical oxidant model, I. An overview of model developments and applications, *Atmos. Environ.*, *25A*, 2077–2090.

Carter, W. P. L. (1996), Condensed atmospheric photooxidation mechanism for isoprene, *Atmos. Environ.*, *30*, 4275–4290.

Carter, W. P. L., and R. Atkinson (1996), Development and evaluation of a detailed mechanism for the atmospheric reactions of isoprene and NO_x, *Int. J. Chem. Kinet.*, *28*, 497–530.

Chameides, W. L., R. D. Saylor, and E. B. Cowling (1997), Ozone pollution in the rural U.S. and the new NAAQS, *Science*, *217*, 916.

Chang, J. S., R. A. Brost, I. S. A. Isaksen, S. Madronich, P. Middleton, W. R. Stockwell, and C. J. Walcek (1987), A three-dimensional Eulerian acid deposition model: Physical concepts and formulation, *J. Geophys. Res.*, *92*, 14,681–14,700.

Chang, J. S., et al. (1990), The Regional Acid Deposition Model and Engineering Model, *NAPAP SOS/T Rep. 4*, in *National Acid Precipitation Assessment Program, Acidic Deposition: State of Science and Technology*, vol. I, pp. 4-1–4-F2, U.S. Govt. Print. Off., Washington, D.C.

Chang, J. S., Y. Li, M. Beauharnois, H.-C. Huang, C.-H. Lu, and G. Wojcik (1996), SAQM user's guide, Calif. Air Resour. Board, Sacramento, Calif.

Chaumerliac, N. (1984), Evaluation des termes de captation dynamique dans un modèle tridimensionel à mesoechelle de lessivage de l'atmosphère, thèse présentée à L'Université de Clermont II, Clermont, France.

Coats, C. J., Jr., A. F. Hanna, D. Hwang, and D. W. Byun (1993), Model engineering concepts for air quality models in an integrated environmental modeling system, paper presented at Specialty Conf. on Regional Photochemical Measurement and Modeling Studies, Air and Waste Manage. Assoc., Pittsburgh, Penn.

DeMore, W. B., S. P. Sander, D. M. Golden, R. F. Hampson, M. J. Kurylo, C. J. Howard, A. R. Ravishankara, C. E. Kolb, and M. J. Molina (1994), Chemical kinetics and photochemical data for use in stratospheric modeling, *Eval. 11, JPL Publ. 94-26*, 273 pp., NASA Jet Propul. Lab., Pasadena, Calif.

Dennis, R. L., J. N. McHenry, W. R. Barchet, F. S. Binkowski, and D. W. Byun (1993), Correcting RADM's sulfate underprediction: Discovery and correction of model errors and testing the corrections through comparisons against field data, *Atmos. Environ.*, *27A*, 975–997.

Dennis, R. L., D. W. Byun, J. H. Novak, K. J. Galluppi, C. J. Coats Jr., and M. A. Vouk (1996), The next generation of integrated air quality modeling: EPA's Models-3, *Atmos. Environ.*, *30*, 1925–1938.

Dodge, M. C. (1989), A comparison of photochemical oxidant mechanisms, *J. Geophys. Res.*, *94*, 5121–5136.

Fiore, A. M., D. J. Jacob, R. Mathur, and R. V. Martin (2003), Application of empirical orthogonal functions to evaluate ozone simulations with regional and global models, *J. Geophys. Res.*, *108*(D14), 4431, doi:10.1029/2002JD003151.

Gery, M. W., G. Z. Whitten, J. P. Killus, and M. C. Dodge (1989), A photochemical kinetics mechanism for urban and regional scale computer modeling, *J. Geophys. Res.*, *94*, 12,925–12,956.

Gilliland, A. B., R. L. Dennis, S. J. Roselle, and T. E. Pierce (2003), Seasonal NH_3 emission estimates for the eastern United States based on ammonium wet concentrations and an inverse modeling method, *J. Geophys. Res.*, *108*(D15), 4477, doi:10.1029/2002JD003063.

Giorgi, F., and W. L. Chameides (1985), The rainout parameterization in a photochemical model, *J. Geophys. Res.*, *90*, 7872–7880.

Grell, G. A., J. Dudhia, and D. R. Stauffer (1994), A description of the fifth-generation Penn State/NCAR Mesoscale Model (MM5), *NCAR Tech. Note NCAR/TN-398+STR*, Natl. Cent. for Atmos. Res., Boulder, Colo.

Hanna, A. F., F. S. Binkowski, and U. Shankar (1993), Analysis of regional visibility in the Eastern United States using aerosol models, paper presented at International Specialty Conference on Regional Photochemical Measurement and Modeling Studies, Air and Waste Manage. Assoc., Pittsburgh, Penn.

Hanna, S. R., A. G. Russell, J. G. Wilkinson, J. Vukovich, and D. A. Hansen (2005), Monte Carlo estimation of uncertainties in BEIS3 emission outputs and their effects on uncertainties in chemical transport model predictions, *J. Geophys. Res.*, *110*, D01302, doi:10.1029/2004JD004986.

Hansen, J., G. Russell, D. Rind, P. Stone, A. Lacis, S. Lebedeff, R. Ruedy, and L. Travis (1983), Efficient three-dimensional global models for climate studies: Models I and II, *Mon. Weather Rev.*, *111*, 609–662.

Harrington, D. Y., and S. M. Kreidenweis (1998), Simulations of sulfate aerosol dynamics—I. Model description, *Atmos. Environ.*, *32*, 1691–1700.

Hogrefe, C., S. T. Rao, P. Kasibhatla, G. Kallos, C. Tremback, W. Hao, D. Olerud, A. Xiu, J. McHenry, and K. Alapaty (2001a), Evaluating the performance of regional-scale photochemical modeling systems: part I. Meteorological predictions, *Atmos. Environ.*, *35*, 4159–4174.

Hogrefe, C., S. T. Rao, P. Kasibhatla, W. Hao, G. Sistla, R. Mathur, and J. McHenry (2001b), Evaluating the performance of regional-scale photochemical modeling systems: part II. Ozone predictions, *Atmos. Environ.*, *35*, 4175–4188.

Houyoux, M. R., J. M. Vukovich, C. J. Coats Jr., N. J. M. Wheeler, and P. S. Kasibhatla (2000), Emission inventory development and processing for the Seasonal Model for Regional Air Quality (SMRAQ) project, *J. Geophys. Res.*, *105*, 9079–9090.

Hübler, G. R., et al. (1998), An overview of the airborne activities during the Southern Oxidants Study (SOS) 1995 Nashville/Middle Tennessee Ozone Study, *J. Geophys. Res.*, *103*, 22,245–22,259.

Kain, J. S., and J. M. Fritsch (1990), A one-dimensional entraining/detraining plume model and its application in convective parameterization, *J. Atmos. Sci.*, *47*, 2784–2802.

Kain, J. S., and J. M. Fritsch (1993), Convective parameterization for mesoscale models: The Kain-Fritsch scheme, in *The Representation of Cumulus Convection in Numerical Models*, *Meteor. Monogr.*, vol. 46, pp. 165–170, Am. Meteor. Soc., Boston, Mass.

Kasibhatla, P., and W. L. Chameides (2000), Seasonal modeling of regional ozone pollution in the eastern United States, *Geophys. Res. Lett.*, *27*, 1415–1418.

Kasibhatla, P., W. L. Chameides, B. Duncan, M. Houyoux, C. Jang, R. Mathur, T. Odman, and A. Xiu (1997), Impact of inert organic nitrate formation on ground-level ozone in a regional air quality model using the Carbon Bond Mechanism 4, *Geophys. Res. Lett.*, *24*, 3205–3208.

Kim, Y. J., and J. F. Boatman (1990), Size calibration corrections for the forward scattering spectrometer probe (FSSP) for measurement of atmospheric aerosols of different refractive indices, *J. Atmos. Oceanic Technol.*, *7*, 681–688.

Koschmieder, H. (1924), Theorie der Horizontalen Sichtweite, *Beitr. Phys. Freinen Atmos.*, *12*, 171–181.

Kumar, N., M. T. Odman, and A. G. Russell (1994), Multiscale air quality modeling: Application to southern California, *J. Geophys. Res.*, *99*, 5385–5397.

Lamb, R. G. (1983), A regional scale (1000 km) model of photochemical air pollution. part I—Theoretical formulation, *EPA-600/3-83-035*, Off. of Res. and Dev., U. S. Environ. Prot. Agency, Washington, D.C.

Lee, Y. N., et al. (1998), Atmospheric chemistry and distribution of formaldehyde and several multioxygenated carbonyl compounds during the 1995 Nashville/Middle Tennessee Ozone Study, *J. Geophys. Res.*, *103*, 22,449–22,462.

Liang, J., and M. Z. Jacobson (2000), Effects of subgrid segregation on ozone production efficiency in a chemical model, *Atmos. Environ.*, *34*, 2975–2982.

Liu, S. C., M. Trainer, F. C. Fehsenfeld, D. D. Parrish, E. J. Williams, D. W. Fahey, G. Hübler, and P. C. Murphy (1987), Ozone production in the rural troposphere and the implications for regional and global ozone distributions, *J. Geophys. Res.*, *92*, 4191–4207.

Lu, R., R. P. Turco, and M. Z. Jacobson (1997), An integrated air pollution modeling system for urban and regional scales: 1. Structure and performance, *J. Geophys. Res.*, *102*, 6063–6079.

Madronich, S. (1987), Photodissociation in the atmosphere: 1. Actinic flux and the effects of ground reflections and clouds, *J. Geophys. Res.*, *92*, 9740–9752.

Malm, W. C., J. F. Sisler, D. Huffman, R. A. Eldred, and T. A. Cahill (1994), Spatial and seasonal trends in particle concentrations and optical extinction in the United States, *J. Geophys. Res.*, *99*, 1347–1370.

Mathur, R., and R. L. Dennis (2003), Seasonal and annual modeling of reduced nitrogen compounds over the eastern United States: Emissions, ambient levels, and deposition amounts, *J. Geophys. Res.*, *108*(D15), 4481, doi:10.1029/2002JD002794.

Mathur, R., L. K. Peters, and R. D. Saylor (1992), Sub-grid representation of emission source clusters in regional air quality modeling, *Atmos. Environ.*, *26A*, 3219–3238.

Mathur, R., J. O. Young, K. L. Schere, and G. L. Gipson (1998), A comparison of numerical techniques for solution of atmospheric kinetic equations, *Atmos. Environ.*, *32*, 1535–1553.

Mathur, R., A. Xiu, A. Hanna, C. Coats Jr., U. Shankar, and J. McHenry (2000), Development, testing, and applications of a regional scale integrated meteorology-atmospheric chemistry model, paper presented at 19th Annual Conference of the American Association for Aerosol Research, St. Louis, Mo., 6–10 November.

McHenry, J. N., and R. L. Dennis (1994), The relative importance of oxidation pathways and clouds to atmospheric ambient sulfate production as predicted by the Regional Acid Deposition Model (RADM), *J. Appl. Meteorol.*, *33*, 890–905.

McHenry, J. N., W. F. Ryan, N. L. Seaman, C. J. Coats Jr., J. Pudykeiwicz, S. Arunachalam, and J. M. Vukovich (2004), A real-time Eulerian photochemical model forecast system: Overview and initial ozone forecast performance in the northeast U.S. corridor, *Bull. Am. Meteorol. Soc.*, *85*, 525–548.

McKeen, S. A., E.-Y. Hsie, M. Trainer, R. Tallamraju, and S. C. Liu (1991), A regional model study of the ozone budget in the eastern United States, *J. Geophys. Res.*, *96*, 10,809–10,845.

McKeen, S. A., G. Wotawa, D. D. Parrish, J. S. Holloway, M. P. Buhr, G. Hübler, F. C. Fehsenfeld, and J. M. Meagher (2002), Ozone production from Canadian wildfires during June and July of 1995, *J. Geophys. Res.*, *107*(D14), 4192, doi:10.1029/2001JD000697.

McNider, R. T., W. B. Norris, A. J. Song, R. L. Clymer, S. Gupta, R. M. Banta, R. J. Zamora, and A. B. White (1998), Meteorological conditions during the 1995 Southern Oxidants Study Nashville/Middle Tennessee field intensive, *J. Geophys. Res.*, *103*, 22,225–22,243.

McRae, G. J., W. R. Goodin, and J. H. Seinfeld (1982), Numerical solution of atmospheric diffusion equation for chemically reactive flows, *J. Comput. Phys.*, *45*, 1–42.

Meagher, J. F., E. B. Cowling, F. C. Fehsenfeld, and W. J. Parkhurst (1998), Ozone formation and transport in the southeastern United States: Overview of the SOS Nashville/Middle Tennessee Ozone Study, *J. Geophys. Res.*, *103*, 22,213–22,224.

Morris, R. E., and T. C. Myers (1990), User's guide for the Urban Airshed Model, Vol. 1, User's manual for UAM (CB-IV), *EPA-450/4-90/007a*, *NTIS PB91-131227/REB*, Natl. Tech. Inf. Serv., Springfield, Va.

Odman, M. T., and A. G. Russell (1991), Multiscale modeling of pollutant transport and chemistry, *J. Geophys. Res.*, *96*, 7363–7370.

Odman, M. T., and A. G. Russell (2000), Mass conservative coupling of non-hydrostatic meteorological models with air quality models, in *Air Pollution Modelling and Its Application XIII*, edited by S. E. Gryning and E. Batchvarova, pp. 651–660, Springer, New York.

Odman, M. T., R. Mathur, K. Alapaty, R. Srivastava, D. S. McRae, and R. J. Yamartino (1997), Nested and adaptive grids for multiscale environmental modeling, in *Next Generation Environmental Models Computational Methods*, edited by G. Delic and M. F. Wheeler, pp. 59–68, Soc. for Indust. and Appl. Math., Philadelphia, Penn.

Pandis, S. N., R. A. Harley, G. R. Cass, and J. H. Seinfeld (1992), Secondary organic aerosol formation and transport, *Atmos. Environ.*, *26A*, 2269–2282.

Pandis, S. N., A. S. Wexler, and J. H. Seinfeld (1993), Secondary organic aerosol formation and transport, 2: Predicting the ambient secondary organic aerosol size distribution, *Atmos. Environ.*, *27*, 2403–2416.

Peters, L. K., et al. (1995), The current state and future direction of Eulerian models in simulating the tropospheric chemistry and transport of trace species: A review, *Atmos. Environ.*, *29*, 189–222.

Pierce, T., C. Geron, L. Bender, R. Dennis, G. Tonnesen, and A. Guenther (1998), Influence of increased isoprene emissions on regional ozone modeling, *J. Geophys. Res.*, *103*, 25,611–25,629.

Pitchford, M. L., and W. C. Malm (1994), Development and application of a standard visual index, *Atmos. Environ.*, *28*, 1049–1054.

Rao, S. T., I. G. Zurbenko, R. Neagu, P. S. Porter, J. Y. Ku, and R. F. Henry (1997), Space and time scales in ambient ozone data, *Bull. Am. Meteorol. Soc.*, *78*, 2153–2166.

Riemer, N., H. Vogel, B. Schell, I. Ackermann, C. Kessler, and H. Hass (2003), Impact of the heterogeneous hydrolysis of N_2O_5 on chemistry and nitrate aerosol formation in the lower troposphere under photosmog conditions, *J. Geophys. Res.*, *108*(D4), 4144, doi:10.1029/2002JD002436.

Russell, A. G., and R. Dennis (2000), NARSTO critical review of photochemical models and modeling, *Atmos. Environ.*, *34*, 2283–2324.

Schere, K. L. (1988), Modeling ozone concentrations, *Environ. Sci. Technol.*, *22*, 488–495.

Seigneur, C., and P. Saxena (1990), Status of subregional and mesoscale models, Vol. 1: Air quality models, *EPRI EN-664*, Elect. Power Res. Inst., Palo Alto, Calif.

Shankar, U., and F. S. Binkowski (1994), Sulfate aerosol wet deposition in a three-dimensional Eulerian air quality modeling framework, paper presented at 4th International Aerosol Conference, Am. Assoc. for Aerosol Res., Cincinnati, Ohio.

Shankar, U., and R. Mathur (2001), Regional modeling of reduced nitrogen species: A comparative analysis of two thermodynamic models, paper presented at 20th Annual Conference, Am. Assoc. for Aerosol Res., Portland, Oreg.

Shankar, U., and R. Mathur (2003), Extending size-dependent composition to the modal approach: A case study with sea salt aerosol, paper presented at the 2nd Annual CMAS Models-3 User's Conference—One Atmosphere, One Community, One Modeling System: Models-3, Environ. Prot. Agency, Research Triangle Park, N.C.

Shankar, U., A. F. Hanna, and S. J. Roselle (1999), Sensitivity of photolysis rates to cloud optical properties in a three-dimensional gas-aerosol model, paper presented at 18th Annual Conference, Am. Assoc. for Aerosol Res., Cincinnati, Ohio.

Sickles, J. E., II (1999), A summary of airborne concentrations of sulfur- and nitrogen-containing pollutants in the northeastern United States, *J. Air Waste Manage. Assoc.*, *49*, 882–893.

Sillman, S., J. A. Logan, and S. C. Wofsy (1990), A regional scale model for ozone in the United States with subgrid representation of urban and power plant plumes, *J. Geophys. Res.*, *95*, 5731–5748.

Sisler, J. F., and W. C. Malm (2000), Spatial distributions of reconstructed light extinctions and light-extinction budgets, in *Spatial and Seasonal Patterns and Temporal Variability of Haze and Its Constituents in the United States*, *Rep. III*, pp. 3-1–3-38, Colo. State Univ., Fort Collins, Colo.

Slinn, W. G. N. (1974), Rate-limiting aspects of in-cloud scavenging, *J. Atmos. Sci.*, *31*, 1172–1173.

Srivastava, R. K., D. S. McRae, and M. T. Odman (1994), Governing equations of atmospheric diffusion, report, MCN, Research Triangle Park, N.C.

Stockwell, W. R., P. Middleton, J. S. Chang, and X. Tang (1990), The second-generation Regional Acid Deposition Model chemical mechanism for regional air quality modeling, *J. Geophys. Res.*, *95*, 16,343–16,367.

Trainer, M., E.-Y. Hsie, S. A. McKeen, R. Tallamraju, D. D. Parrish, F. C. Fehsenfeld, and S. C. Liu (1987), Impact of natural hydrocarbons on hydroxyl and peroxy radicals at a remote site, *J. Geophys. Res.*, *92*, 11,879–11,894.

U.S. Environmental Protection Agency (1991), Guidelines for regulatory applications of the Urban Airshed Model, *EPA-450/4-91-013*, Off. of Air Quality Plan. and Stand., Research Triangle Park, N.C.

Venkatram, A., P. K. Karamchandani, and P. K. Misra (1988), Testing a comprehensive acid deposition model, *Atmos. Environ.*, *22*, 737–747.

Vukovich, J., and T. Pierce (2002), The implementation of BEIS3 within the SMOKE modeling framework, paper presented at the Emissions Inventory Conference, Environ. Prot. Agency, Atlanta, Ga.

Walcek, C. J., and G. R. Taylor (1986), A theoretical model for computing vertical distributions of acidity and sulfate production within cumulus clouds, *J. Atmos. Sci.*, *43*, 339–355.

Wamsley, J. L., and M. L. Wesely (1996), Modification of coded parameterizations of surface resistances to gaseous dry deposition, *Atmos. Environ.*, *30*, 1181–1188.

Whitby, E. R., P. H. McMurray, U. Shankar, and F. S. Binkowski (1991), Modal aerosol dynamics modeling, *EPA/60013-91/020 (NTIS PB91-161729/AS)*, Natl. Tech. Inf. Serv., Springfield, Va.

Wiscombe, W. J. (1980), Improved Mie scattering algorithms, *Appl. Opt.*, *19*, 1505–1509.

Wotawa, G., and M. Trainer (2000), The influence of Canadian forest fires on pollutant concentrations in the United States, *Science*, *288*, 324–328.

Xu, K.-M., and S. K. Krueger (1991), Evaluation of cloudiness using a cumulus ensemble model, *Mon. Weather Rev.*, *119*, 342–367.

Yamartino, R. J., J. S. Scire, G. R. Carmichael, and Y. S. Chang (1992), The CALGRID mesoscale photochemical grid model, Part I. Model formulation, *Atmos. Environ.*, *26A*, 1493–1512.

Yanenko, N. N. (1971), *The Method of Fractional Steps*, Springer, New York.

K. Alapaty, S. Arunachalam, F. S. Binkowski, A. F. Hanna, U. Shankar, and A. Xiu, Carolina Environmental Program, University of North Carolina at Chapel Hill, CB 6116, Chapel Hill, NC 27599-6116, USA.

D. W. Byun, University of Houston, Houston, TX 77204, USA.

J. K. S. Ching, R. L. Dennis, R. Mathur, T. E. Pierce, J. E. Pleim, S. J. Roselle, K. L. Schere, and J. O. Young, Atmospheric Sciences Modeling Division, Air Resources Laboratory, National Oceanic and Atmospheric Administration, Research Triangle Park, NC 27711, USA. (rohit.mahur@noaa.gov)

C. J. Coats Jr., J. N. McHenry, and D. T. Olerud Jr., Baron Advanced Meteorological Systems, c/o North Carolina State University, 920 Main Campus Drive, Raleigh, NC 27606, USA.

M. T. Odman, Georgia Institute of Technology, Atlanta, GA 30332, USA.